

1 **FBXO47 is essential for preventing the synaptonemal complex from premature**  
2 **disassembly in mouse male meiosis**

3

4 Nobuhiro Tanno<sup>1,4</sup>, Kazumasa Takemoto<sup>1,4</sup>, Yuki Takada-Horisawa<sup>1</sup>, Ryuki Shimada<sup>1</sup>, Sayoko  
5 Fujimura<sup>2</sup>, Naoki Tani<sup>2</sup>, Naoki Takeda<sup>3</sup>, Kimi Araki<sup>3</sup> and Kei-ichiro Ishiguro<sup>1,5\*</sup>

6

7 1 Department of Chromosome Biology, Institute of Molecular Embryology and Genetics  
8 (IMEG), Kumamoto University, Kumamoto, 860-0811 Japan

9 2 Liaison Laboratory Research Promotion Center, IMEG, Kumamoto University

10 3 Institute of Resource Development and Analysis and Center for Metabolic Regulation  
11 of Healthy Aging, Kumamoto University, Kumamoto, 860-0811 Japan

12 4 These authors equally contributed

13 5 Lead contact

14 \* correspondence : [ishiguro@kumamoto-u.ac.jp](mailto:ishiguro@kumamoto-u.ac.jp)

15

16 **Abstract**

17 **Meiotic prophase is a prolonged G2 phase that ensures the completion of numerous**  
18 **meiosis-specific chromosome events. During meiotic prophase, homologous chromosomes**  
19 **undergo synapsis to facilitate meiotic recombination yielding crossovers. It remains**  
20 **largely elusive how homolog synapsis is temporally maintained and destabilized during**  
21 **meiotic prophase. Here we show that FBXO47 is the stabilizer of synaptonemal complex**  
22 **during male meiotic prophase. Disruption of FBXO47 shows severe impact on homologous**  
23 **chromosome synapsis and DSB repair processes, leading to male infertility. Notably, in the**  
24 **absence of FBXO47, although once homologous chromosomes are synapsed, the**  
25 **synaptonemal complex is precociously disassembled before progressing beyond pachytene.**  
26 **Remarkably, *Fbxo47* KO spermatocytes remain in earlier stage of meiotic prophase and**  
27 **lack crossovers, despite apparently exhibiting diplotene-like chromosome morphology. We**  
28 **propose that FBXO47 functions independently of SCF E3 ligase, and plays a crucial role**  
29 **in preventing synaptonemal complex from premature disassembly during cell cycle**  
30 **progression of meiotic prophase.**

31

32

33 **Introduction**

34 Meiosis consists of a single DNA replication followed by two rounds of chromosome  
35 segregation, which halves the chromosome number to ultimately produce haploid gametes.

36 During meiotic prophase I, sister chromatids are organized into proteinaceous structures, termed  
37 axial element (AE) or chromosome axis (Zickler and Kleckner, 2015). Homologous  
38 chromosomes (homologs) then undergo synapsis, which is promoted by the assembly of  
39 synaptonemal complex (SC) (Cahoon and Hawley, 2016). Homolog synapsis facilitates meiotic  
40 recombination yielding crossovers, a process that produces physical linkages called chiasmata  
41 between the homologs (Baudat et al., 2013) (Keeney et al., 2014). While homolog synapsis  
42 persists until meiotic recombination is completed during pachytene, it is dissolved upon  
43 diplotene-Metaphase I transition. Thus, homolog synapsis and de-synapsis is temporally  
44 regulated. However, it remains elusive how homolog synapsis is temporally maintained and  
45 destabilized during meiotic prophase.

46 SCF (SKP1–Cullin–F-box) E3 ubiquitin ligase is a key regulator of cell cycle (Deshaies, 1999)  
47 (Cardozo and Pagano, 2004). Accumulating lines of evidence suggest that SCF is involved in  
48 homolog synapsis in a wide variety of organisms. In mouse, homologous chromosomes showed  
49 premature desynapsis in *Skp1* conditional KO spermatocytes (Guan et al., 2020), suggesting that  
50 SCF is required for the maintenance of SC during male meiotic prophase. In *Drosophila* female,  
51 SkpA, a SKP1 homolog, is required for the assembly and/or the maintenance of SC (Barbosa et  
52 al., 2021). In budding yeast *Saccharomyces cerevisiae*, depletion of *Cdc53* that encodes Cullin  
53 resulted in defects in SC formation (Zhu et al., 2021). Thus, SCF is involved in the process of  
54 homolog synapsis during meiotic prophase in diverse organisms.

55 Fbox-domain containing proteins act as a substrate recognition subunit in SCF E3 ubiquitin  
56 ligase (Kipreos and Pagano, 2000) (Jin et al., 2004) (Reitsma et al., 2017). It has been shown  
57 that Fbox-domain containing proteins are involved in homolog synapsis in a wide variety of  
58 organisms. In rice plant *Oryza sativa*, mutants of MEIOTIC F-box *MOF* (He et al., 2016) and  
59 another Fbox *ZYGO1* (Zhang et al., 2017) showed defects in DNA double-strand break (DSB)  
60 repair and bouquet formation during meiotic prophase. In budding yeast, temperature sensitive  
61 mutant of *Cdc4* that encodes F-box protein showed defective SC formation and DSB repair  
62 (Zhu et al., 2021). In *Drosophila* female, depletion of Slmb ( $\beta$ Trcp) and CG6758 (Fbxo42)  
63 caused impaired assembly and/or premature disassembly of SC (Barbosa et al., 2021). Although  
64 the substrates are yet to be indentified in most of the cases, Fbox-domain containing proteins  
65 directly or indirectly regulate the assembly and disassembly of SC.

66  
67 Previously, we identified MEIOSIN that plays an essential role in meiotic initiation both in  
68 mouse male and female (Ishiguro et al., 2020). MEIOSIN together with STRA8 (Kojima et al.,  
69 2019) activates meiotic genes and directs the switching from mitosis to meiosis. In the present  
70 study, we identified *Fbxo47* gene that encodes a Fbox protein, as one of the  
71 MEIOSIN/STRA8-target genes. Previous genetic studies suggested FBXO47 homologs are  
72 implicated in the progression of meiotic prophase in different species. In *C. elegance*, mutation  
73 in *prom-1* that encodes putative *Fbxo47* homolog, showed reduced homologous chromosome  
74 pairing and bivalent formation (Jantsch et al., 2007). In medaka fish, *fbxo47* mutant fails to  
75 complete meiotic prophase in female but switches developmental fate from oogenesis into  
76 spermatogenesis (Kikuchi et al., 2020). In mouse, *Fbxo47* gene that has previously been

77 identified as a meiotic gene by single cell RNA-seq analysis of testes, is essential for mouse  
78 spermatogenesis (Chen et al., 2018) (Hua et al., 2019). Although previous studies suggest that  
79 FBXO47 homologs and distant meiotic Fbox-domain containing proteins play a role in  
80 homologous chromosome pairing/synapsis and meiotic recombination in a wide variety of  
81 organisms, the precise mechanisms how these proteins are involved in these processes remained  
82 elusive. Furthermore, whether FBXO47 is indeed involved in the function of SCF is unknown.  
83 Here we show that mouse FBXO47 is essential for maintaining homolog synapsis during  
84 meiotic prophase. FBXO47 is a cytoplasmic protein rather than a telomere binding protein, and  
85 functions independently of SCF. We demonstrate that in *Fbxo47* KO spermatocytes,  
86 homologous chromosome synapsis is complete, but SC is precociously disassembled. Further,  
87 we show that *Fbxo47* KO spermatocytes fail to progress beyond pachytene and remain in earlier  
88 meiotic prophase in terms of cell cycle progression, despite the apparent exhibition of  
89 diplotene-like morphology of chromosomes. We propose that FBXO47 is essential for  
90 preventing SC from premature destruction during cell cycle progression of male meiotic  
91 prophase. Further, we discuss the different observations and interpretations between the present  
92 study and the previous study on FBXO47 (Hua *et al.*, 2019).

93

## 94 **Results**

### 95 **FBXO47 is expressed in mouse testes**

96 Previously, we demonstrated that MEIOSIN collaborating with STRA8 activates meiotic genes,  
97 which are required for numerous meiotic events (Ishiguro *et al.*, 2020). In spermatocytes, we  
98 identified *Fbxo47* as one of the MEIOSIN/STRA8-bound genes (Fig. 1A). Our previous  
99 RNA-seq analysis showed that expression of *Fbxo47* was significantly downregulated in  
100 *Meiosin* KO testes at postnatal day 10 (P10) when a cohort of spermatocytes should undergo the  
101 first wave of meiotic entry (Ishiguro *et al.*, 2020). We confirmed this by RT-qPCR analysis  
102 demonstrating that *Fbxo47* expression level was indeed downregulated in *Meiosin* KO testis at  
103 P10 (Fig. 1B). We further examined the expression patterns of *Fbxo47* in different mouse  
104 tissues by RT-PCR analysis. *Fbxo47* gene showed higher expression levels in adult testis  
105 compared to other adult organs that we examined (Fig. 1C). Spermatogenic expression of  
106 *Fbxo47* gene was further confirmed by the reanalysis of previous scRNA-seq data of adult  
107 mouse testis (Hermann *et al.*, 2018) (Fig. 1D). The result indicated that *Fbxo47* was  
108 coordinately expressed with the landmark genes of meiotic spermatocyte such as *Dmc1*, and  
109 spermatid at spermiogenesis such as *Acrv1*, rather than those of spermatogonia such as *Zbtb16*  
110 (Fig. 1D). We noticed that *Fbxo47* mRNA was expressed weakly in meiotic spermatocytes, and  
111 highly in spermatids in testes, which is consistent with a previous study (Chen *et al.*, 2018). In  
112 females, expression of *Fbxo47* mRNA was examined by the reanalysis of previous scRNA-seq  
113 data of fetal ovaries (Shimada *et al.*, 2021). We found that *Fbxo47* was coordinately expressed  
114 during meiotic prophase, such as *Dmc1* (Fig. 1E). Expression of *Fbxo47* mRNA culminated  
115 at E16.5 and declined afterward in the ovary (Fig. 1F).

116 To determine the meiotic stage-specific expression of FBXO47 protein, we generated different  
117 antibodies against FBXO47 C-terminal region (aa 271- 451) and middle region (aa173-316).

118 However, we failed to evaluate stage specificity of endogenous FBXO47 protein expression by  
119 immunostaining, although it was uncertain whether this was due to the sensitivity of the  
120 antibodies, inaccessibility of the antibodies to the epitopes, or low expression level of FBXO47  
121 protein in the target cells.  
122 To circumvent this issue, we generated *Fbxo47-3xFLAG-HA* knock-in (*Fbxo47-3FH-GFP* KI)  
123 mice, which allowed the detection of FBXO47-3xFLAG-HA protein expressed from  
124 endogenous *Fbxo47* locus (Fig. 1G, Fig. S1). We examined FBXO47-3xFLAG-HA fusion  
125 protein from cytosolic and chromatin extracts of *Fbxo47-3FH-GFP* KI testes. Immunoblotting  
126 demonstrated that FBXO47 protein was detected with FLAG antibody only when it was  
127 enriched by tandem immunoprecipitations using anti-FLAG and anti-HA antibodies (Fig. 1H),  
128 suggesting that the expression level of FBXO47 protein was low in testes. We noticed that more  
129 FBXO47 protein was detected in the cytosolic fraction compared to the chromatin fraction (Fig.  
130 1H), suggesting its predominant localization in the cytoplasm rather than on the chromatin.  
131 Sequential reblotting showed that different antibodies against the endogenous FBXO47 protein  
132 that we generated detected the same protein as indicated by anti-FLAG antibody (Fig. 1H).  
133 Previous study showed that FBXO47 binds to telomeric proteins TRF1 and TRF2 (Hua *et al.*,  
134 2019). However, we failed to detect neither TRF1 nor TRF2 in FBXO47 immunoprecipitates  
135 from testis chromatin fraction (Fig. S3A), which was a sharp contrast to the previous study (Hua  
136 *et al.*, 2019).

137

### 138 **FBXO47 may function independently of SCF in spermatocytes.**

139 FBXO47 possesses a putative Fbox domain, whose biological function has remained elusive. It  
140 is well known that Fbox-domain containing proteins confers substrate specificity to SCF  
141 (SKP1–Cullin–F-box) E3 ubiquitin ligase (Jin *et al.*, 2004), and 69 different Fbox proteins are  
142 estimated to be encoded in human genome (Reitsma *et al.*, 2017). This prompted us to examine  
143 whether SKP1, a major core subunit of SCF, was co-immunoprecipitated with FBXO47 by  
144 immunoblot and mass spectrometry analysis (Fig. 1H, Fig. S2). However, we failed to detect  
145 SKP1 in FBXO47 immunoprecipitates.

146 To further examine whether FBXO47 serves as a subunit of SCF by reciprocal  
147 immunoprecipitation of SKP1, we generated *Skp1-3xFLAG-HA* knock-in (*Skp1-3FH-GFP* KI)  
148 mice, which allowed the detection of SKP1-3xFLAG-HA protein expressed from endogenous  
149 *Skp1* locus and its associated factors (Fig. 2A). Although the homozygous *Skp1-3xFLAG-HA* KI  
150 mice were embryonic lethal, heterozygous knock-in mice were fertile and developed normally.  
151 Consistent with a previous study (Guan *et al.*, 2020), SKP1-3xFLAG-HA fusion protein  
152 localized along the SC in the *Skp1-3FH-GFP* KI spermatocytes (Fig. 2B). SKP1-3xFLAG-HA  
153 was enriched by tandem immunoprecipitations using anti-FLAG and anti-HA antibodies from  
154 testis cytosolic fraction (Fig. 2C). Mass spectrometry analysis demonstrated that total of 45  
155 different Fbox-domain containing proteins and SCF core subunits (SKP1, RBX1, CUL1, CUL7)  
156 were co-immunoprecipitated with SKP1-3xFLAG-HA (Fig. 2D, Supplementary Data1).

157 However, we failed to detect FBXO47 in the SKP1-3xFLAG-HA immunoprecipitates either by  
158 mass spectrometry analysis or by western blotting (Fig. 2D, E). SKP1 localized along the SC in

159 *Fbxo47* KO, suggesting that localization of SKP1 did not depend on FBXO47 (Fig. 2F).  
160 Altogether, our data suggest that FBXO47 may function independently of SCF in mouse testes.  
161 Previous study showed that FBXO47 interacts with SKP1 in yeast two hybrid assay and in  
162 GFP-SKP1 IP using HEK293T cell extract that overexpressed FLAG-FBXO47 and  
163 GFP-SKP1 (Hua *et al.*, 2019). Although we do not know the exact reason for these controversial  
164 observations between our present study and the previous one (Hua *et al.*, 2019), this could be  
165 due to their detection methodology using yeast and overexpression of FBXO47 in culuture cells.  
166

### 167 **Expression of FBXO47 is limited to early meiotic prophase in mouse testes**

168 To identify the specific stage in which FBXO47 was expressed, we performed immunostaining  
169 using stage specific markers SYCP3 (a component of meiotic chromosome axis), SYCP1 (a  
170 marker of homologous chromosome synapsis), and  $\gamma$ H2AX (a marker of DSBs).  
171 Immunostaining of the *Fbxo47-3FH-GFP* KI testis (P15) indicated that FBXO47 protein was  
172 detected by HA antibody in average 21% (n = 3) among total SYCP3 positive seminiferous  
173 tubules (Fig. 3A). Close inspection of seminiferous tubules showed that FBXO47 protein  
174 indicated by the presence of HA staining appeared in the cytosol at leptotene and zygotene (Fig.  
175 3B, C). Notably, the expression level of FBXO47-3xFLAG-HA fusion protein declined in  
176 pachyete, when homologs were fully synapsed (Fig. 3C). Testis-specific histone H1t is a  
177 marker of spermatocytes later than mid pachyete (Cobb *et al.*, 1999) (Drabent *et al.*, 1996).  
178 Immunostaining of seminiferous tubules by testis-specific histone H1t indicated that FBXO47  
179 protein was expressed only in H1t negative stage (Fig. 3D). None of H1t positive spermatocytes  
180 showed FBXO47 immunostaining (Fig. 3E), suggestiung that FBXO47 expression had declined  
181 by mid-pachyete. Thus, the expression of FBXO47 protein was limited to a narrow window of  
182 early meiotic prophase. Although the expression of *Fbxo47* mRNA was upregulated in  
183 spermatids, immunostaining of FBXO47 protein detected no more than background levels in  
184 spermatids (Fig. 3F). This suggested that the expression of FBXO47 might be  
185 post-transcriptionally suppressed after post-meiotic spermatids to have the expression  
186 specifically limited to early meiotic prophase.

187

188

### 189 **Disruption of *Fbxo47* led to severe defect in spermatogenesis**

190 In order to address the role of *Fbxo47* in meiosis, we deleted Exon3-Exon11 of *Fbxo47* loci in  
191 C57BL/6 fertilized eggs through the CRISPR/Cas9 system (Fig. 4A). RT-PCR analysis showed  
192 that *Fbxo47* mRNA expression level was absent in *Fbxo47* KO testis (Fig. 4B). Although  
193 *Fbxo47* KO male mice did not show overt phenotype in somatic tissues, defects in male  
194 reproductive organs were evident with smaller-than-normal testes (Fig. 4C). Histological  
195 analysis revealed that post-meiotic spermatids and spermatozoa were absent in eight-week-old  
196 *Fbxo47* KO seminiferous tubules (Fig. 4D). Accordingly, sperm was absent in adult *Fbxo47* KO  
197 caudal epididymis (Fig. 4E). Consistently, seminiferous tubules that contain PNA lectin (a  
198 marker of spermatids) positive cells were absent in *Fbxo47* KO (Fig. 4F). Thus, the later stage  
199 of spermatogenesis was severely abolished in *Fbxo47* KO seminiferous tubules, resulting in

200 male infertility (Fig. 4G). In contrast to male, *Fbxo47* KO females exhibited seemingly normal  
201 fertility with no apparent defects in adult ovaries (Fig. 4H). Consistent with this histological  
202 observation of ovaries, metaphase I oocytes derived from *Fbxo47* KO females processes normal  
203 number of bivalent chromosomes with chiasmata, indicating that *Fbxo47* KO oocytes had  
204 progressed normal meiotic prophase (Fig. 4I). Furthermore, *Fbxo47* KO females were fertile  
205 (Fig. 4G, J), although we could not exclude the possibility that more subtle defects might have  
206 occurred in the ovaries besides fertility. Thus, the infertility caused by disruption of *Fbxo47* was  
207 male specific. Therefore, these results suggest that requirement of FBXO47 is sexually different  
208 in mouse.

209

### 210 **Synaptonemal complex was prematurely disassembled in *Fbxo47* KO spermatocytes.**

211 To further investigate at which stage the primary defect appeared in the *Fbxo47* KO, we  
212 analyzed the progression of spermatogenesis by immunostaining. Testis-specific histone H1t is  
213 a marker of spermatocytes later than mid pachytene and round spermatids (Cobb *et al.*, 1999)  
214 (Drabent *et al.*, 1996). Close inspection of the seminiferous tubules (3 week) by  
215 immunostaining with antibodies against H1t along with SYCP3 (a component of meiotic  
216 chromosome axis) indicated that *Fbxo47* KO spermatocytes failed to reach mid pachytene,  
217 whereas spermatocytes in age-matched control passed beyond mid pachytene as indicated by  
218 the presence of H1t staining (Fig. 5A). This suggests that progression of meiotic prophase was  
219 blocked in *Fbxo47* KO spermatocytes. Immunostaining analysis of spread chromosome with  
220 antibodies against SYCP3 along with SYCP1 (a marker of homolog synapsis) demonstrated that  
221 *Fbxo47* KO spermatocytes underwent homologous chromosome synapsis and seemingly  
222 reached pachytene stage as in age-matched control (Fig. 5B).

223 Curiously, however, *Fbxo47* KO spermatocytes exhibited apparent diplotene-like chromosome  
224 morphology, despite the failure in reaching H1t positive mid pachytene (Fig. 5A). It is known  
225 that homolog synapsis is initiated at interstitial regions on the chromosome arm at zygotene, and  
226 that de-synapsis of homologs first starts at interstitial regions on the chromosome arm, while  
227 telomere regions are prone to be the last place of de-synapsis at diplotene (Bisig *et al.*, 2012)  
228 (Qiao *et al.*, 2012). This cytological difference readily distinguishes de-synapsed chromosomes  
229 at diplotene from un-synapsed ones at zygotene. Indeed, those *Fbxo47* KO spermatocytes with  
230 diplotene-like chromosome morphology apparently showed a typical feature of de-synapsis of  
231 homologs, wherein telomere regions retained homolog synapsis while interstitial regions were  
232 free from synapsis. To solve the paradox that *Fbxo47* KO spermatocytes showed diplotene-like  
233 chromosome morphology despite the failure of progressing beyond H1t-positive pachytene  
234 stage, we further analyzed the meiotic prophase population at P15 and P18 in the first wave of  
235 spermatogenesis of *Fbxo47* KO testes. Notably, diplotene-like cells (6.7 %) appeared in *Fbxo47*  
236 KO spermatocytes as early as P15, whereas the first wave of spermatogenesis was yet to pass  
237 beyond pachytene stage in the age-matched WT (Fig. 5C). HORMAD1 localizes along  
238 un-synapsed chromosomes before pachytene and de-synapsed chromosomes at diplotene, but  
239 dissociates from synapsed chromosomes (Shin *et al.*, 2010) (Daniel *et al.*, 2011) (Wojtasz *et al.*,  
240 2009). In *Fbxo47* KO spermatocytes, HORMAD1 dissociated from synapsed chromosomes at

241 pachytene and re-localizes on de-synapsed chromosomes at diplotene-like stage as in those of  
242 WT (Fig. 5D), suggesting that localization of HORMAD1 on chromosomes was normally  
243 regulated. Histone H3 Ser10 phosphorylation (H3S10p) by Aurora B kinase of the chromosome  
244 passenger complex marks the centromeric region at diplotene and the whole chromosome at  
245 metaphase I (Parra et al., 2009) (Parra et al., 2003). In the control spermatocytes, the  
246 centromeric regions at diplotene were indicated by immunostaining of H3S10p (Fig. 5E). In  
247 contrast, H3S10p-positive centromeric regions were not observed in *Fbxo47* KO diplotene-like  
248 spermatocytes (Fig. 5E). This observation indicated that *Fbxo47* KO spermatocytes failed to  
249 reach *bona fide* diplotene stage of meiotic prophase, albeit exhibiting apparent homolog  
250 de-synapsis. Thus, we reasoned that even though homolog synapsis once occurred, it was  
251 destabilized during pachytene in *Fbxo47* KO spermatocytes. It should be mentioned that more  
252 zygotene and reciprocally less pachytene populations were observed in *Fbxo47* KO  
253 spermatocytes compared to WT at P15 and P18 (Fig. 5C). This implies that the process of  
254 homolog synapsis, at least in part, may be delayed in *Fbxo47* KO spermatocytes.

255  
256 Mid-late pachytene spermatocytes acquire competency for meiotic prophase-Metaphase I  
257 transition indicated by the response to phosphatase inhibitor okadaic acid (OA) (Cobb *et al.*,  
258 1999). *In vitro* culture of isolated spermatocytes in the absence or presence of OA demonstrated  
259 that while the control spermatocytes progressed to diakinesis/metaphase I in the presence of OA,  
260 *Fbxo47* KO spermatocytes did not (Fig. 5F). Since *Fbxo47* KO spermatocytes were yet to  
261 acquire competency for OA-induced progression into metaphase I, even the most advanced  
262 *Fbxo47* KO spermatocytes remained in an earlier cell cycle stage compared to the control.  
263 These results suggested that the primary defect occurred at zygotene or early pachytene stage in  
264 *Fbxo47* KO spermatocytes. Notably, TUNEL positive cells were observed in ~21% of *Fbxo47*  
265 KO seminiferous tubules (Fig. 5G), suggesting that *Fbxo47* KO spermatocytes were  
266 consequently eliminated by apoptosis. Altogether, these results suggested that SC was  
267 prematurely disassembled in *Fbxo47* KO spermatocytes (Fig. 5H).

### 268 269 ***Fbxo47* KO spermatocytes show defects in meiotic recombination**

270 Aforementioned results suggested that FBXO47 protein was required for stable maintenance of  
271 SC (Fig. 5). SC facilitates meiotic recombination that is executed by DSB formation and repair  
272 steps. Then SC is disassembled after the completion of crossover formation. Given that SC was  
273 prematurely destabilized in *Fbxo47* KO spermatocytes, we assumed two possibilities: (1)  
274 premature SC disassembly could be a result of early completion of meiotic recombination. (2)  
275 premature SC disassembly abolished the processes of meiotic recombination. To address these  
276 issues, we examined DSB formation and repair events by immunostaining of  $\gamma$ H2AX. The first  
277 wave of  $\gamma$ H2A is mediated by ATM after DSB formation at leptotene (Mahadevaiah *et al.*,  
278 2001), and disappears during DSB repair. The second wave of  $\gamma$ H2A at zygotene is mediated by  
279 ATR that targets unsynapsed chromosomes (Royo *et al.*, 2013). At zygotene,  $\gamma$ H2AX signal  
280 appeared in *Fbxo47* KO spermatocytes in the same manner as WT (Fig. 6A), indicating that  
281 DSB formation normally occurred in *Fbxo47* KO spermatocytes. However,  $\gamma$ H2AX signals

282 largely persisted throughout the nuclei until pachytene-like and diplotene-like stages in *Fbxo47*  
283 KO spermatocytes, while they overall disappeared in WT pachytene spermatocytes except for  
284 retaining on the XY body (Fig. 6A). This observation suggested that DSB was still not repaired  
285 in *Fbxo47* KO diplotene-like spermatocytes. Furthermore, BRCA1, a marker of asynapsis  
286 (Scully et al., 1997) (Turner et al., 2004) (Broering et al., 2014), appeared along unsynapsed  
287 autosomal axes in zygotene *Fbxo47* KO spermatocytes as in those of WT (Fig. 6B). This  
288 suggests that meiotic silencing of unsynapsed chromatin (MUSC) was normally activated in  
289 *Fbxo47* KO spermatocytes. Crucially, in contrast to un-synapsed chromosomes in zygotene,  
290 BRCA1 was not observed along precociously de-synapsed chromosomes in *Fbxo47* KO  
291 diplotene-like spermatocytes (Fig. 6B). This suggests that MUSC was canceled in *Fbxo47* KO  
292 diplotene-like spermatocytes, presumably once homolog synapsis had successfully been  
293 achieved.

294 RAD51 facilitates the invasion of 3'-extended strand into the duplex of homolog at DSBs  
295 (Cloud et al., 2012) (Shinohara and Shinohara, 2004). In accordance with the persistent DSBs in  
296 *Fbxo47* KO (Fig. 6A), the number of RAD51 foci was significantly increased in *Fbxo47* KO  
297 spermatocytes (Fig. 6C). Reciprocally, the number of MSH4 foci was decreased in *Fbxo47* KO  
298 spermatocytes (Fig. 6D). These observations suggest that although RAD51 was normally loaded  
299 onto DSBs, the processes of homologous recombination-mediated repair were delayed or  
300 blocked in the absence of FBXO47. Accordingly, the number of MLH1 foci, a marker of  
301 crossover (CO), was significantly reduced in *Fbxo47* KO pachytene-like spermatocytes  
302 compared to WT pachytene spermatocytes (Fig. 6E). This implies that crossover recombination  
303 was incomplete in the absence of FBXO47. Altogether, precocious disassembly of SC was a  
304 cause of the defect in meiotic recombination rather than a result of early completion of meiotic  
305 recombination.

306  
307

## 308 Discussion

### 309 FBXO47 stabilizes homolog synapsis independently of SCF in mouse

310 We have shown that FBXO47 is required for the maintenance of homolog synapsis during  
311 prolonged meiotic prophase. *Fbxo47* KO spermatocytes showed precocious de-synapsis, albeit  
312 exhibiting apparently “diplotene-like” morphology (Fig. 5B). Although this phenomenon in  
313 *Fbxo47* KO spermatocytes was partly similar to that observed in conditional *Skp1* KO (Guan *et*  
314 *al.*, 2020), marked phenotypic differences were observed between *Fbxo47* KO and *Skp1* KO  
315 spermatocytes. In *Skp1* KO testis, late pachytene spermatocytes are absent and concurrently  
316 diplotene spermatocytes are increased. *Skp1* KO spermatocytes at least reach H1t positive  
317 mid-pachytene in terms of cell cycle, but most of them contain de-synapsed chromosomes at  
318 pericentric end termed “Y pachynema”. Thus, *Skp1* KO spermatocytes show precocious  
319 de-synapsis and pachytene exit. In contrast, *Fbxo47* KO spermatocytes failed to reach H1t  
320 positive mid-pachytene (Fig. 5A). Although apparent diplotene-like morphology of homolog  
321 chromosomes appeared in *Fbxo47* KO spermatocytes (Fig. 5B), “Y pachynema” was not  
322 observed in *Fbxo47* KO, unlike in *Skp1* KO spermatocytes. Thus, *Fbxo47* KO spermatocytes



323 show precocious desynapsis despite the failure of progression beyond pachytene. These results  
324 suggested that primary defect in *Fbxo47* KO spermatocyte occurred at earlier cell cycle stage  
325 than *Skp1* KO spermatocytes. HORMAD1 localizes along unsynapsed and de-synapsed  
326 chromosomes during meiotic prophase (Shin *et al.*, 2010) (Daniel *et al.*, 2011), and dissociates  
327 from synapsed chromosomes by the action of TRIP13 AAA ATPase (Wojtasz *et al.*, 2009).  
328 Whereas HORMAD1 persists both in synapsed and desynapsed chromosomes in *Skp1* KO  
329 spermatocyte, localization of HORMAD1 on chromosomes was normally regulated in *Fbxo47*  
330 KO (Fig. 5D). Thus, precocious desynapsis could be derived at least in part from failure of  
331 HORMAD1 removal in *Skp1* KO and from different mechanism in *Fbxo47* KO. Moreover,  
332 while DSB repair process indicated by  $\gamma$ H2AX staining (Fig. 6A) was impaired both in *Fbxo47*  
333 KO and in *Skp1* KO spermatocytes, the extent of crossover formation was different between  
334 them. Whereas significant number of MLH1 foci were observed in mid-late pachytene and  
335 diplotene spermatocytes in *Skp1* KO, MLH1 foci were rarely observed in pachytene and  
336 diplotene-like spermatocytes in *Fbxo47* KO (Fig. 6E). Thus, meiotic recombination and  
337 crossover formation were more progressed in *Skp1* KO than in *Fbxo47* KO.

338  
339 Fbox-domain containing proteins confers substrate specificity to SCF E3 ubiquitin ligase (Jin *et al.*  
340 *et al.*, 2004) (Reitsma *et al.*, 2017). Although FBXO47 possesses a putative Fbox domain, it was  
341 not detected in the SKP1 immunoprecipitates from *Skp1-3xFLAG-HA* KI testes (Fig. 2D,  
342 Supplementary Data1). Reciprocally, SKP1 was not detected in the immunoprecipitates from  
343 *Fbxo47-3xFLAG-HA* KI testes (Fig. 1H, Fig S2). Furthermore, while SKP1 localized along  
344 lateral element (LE) of synapsed chromosomes (Fig. 2B) (Guan *et al.*, 2020), FBXO47 protein  
345 did not show such a specific localization pattern on the chromosome (Fig. S3B). Although we  
346 cannot formally exclude a possibility that FBXO47 is incorporated as a substrate recognition  
347 subunit in SCF under specific regulation, our results suggest that FBXO47 may not be  
348 incorporated in the function of SCF, and rather FBXO47 may function independently of SCF  
349 in spermatocytes.

350

### 351 **Distinct functions of FBXO47 homologs in diverse organisms**

352 *Fbxo47* homologues and other distant F-box proteins have been implicated in meiotic prophase  
353 progression in various species. Although defects accompanying DSB repair and crossover are  
354 similarly observed in mouse and *C. elegans Fbxo47* mutants, the primary causes are assumed to  
355 be different. In *C. elegans*, PROM-1 encodes *Fbxo47* homolog. In *C. elegans*, organization of  
356 gonadal germline is divided into mitotic/meiotic entry zone, transition zone corresponding to  
357 zygotene, and pachytene zone. *Prom-1* mutant showed delayed and asynchronous initiation of  
358 homolog pairing, so that distinct transition zone was missing and meiotic entry zone was rather  
359 extended (Jantsch *et al.*, 2007) with attenuating CHK-2 activity (Mohammad *et al.*, 2018)  
360 (Baudrimont *et al.*, 2021). Further, PROM-1 was proposed to down regulate mitotic cell cycle  
361 proteins such as Cyclin E homolog CYE-1 at meiotic entry, independently of promoting  
362 homolog pairing as a positive regulator of CHK-2 kinase (Mohammad *et al.*, 2018). Thus,  
363 PROM-1 functions very early in meiotic prophase in *C. elegans*, which is similar to our

364 observation in mice (Fig. 5). In *prom-1* meicytes however, homolog pairing was defective and  
365 non-homologous synapsis was consequently pronounced in autosomes but not in X  
366 chromosome. Thus, PROM-1 is implicated in promoting autosome homolog pairing. This is a  
367 contrast to our observation, in which homolog synapsis once took place normally, followed by  
368 premature desynapsis in *Fbxo47* KO spermatocytes (Fig. 5B).

369 In the teleost fish medaka, *fbxo47* mutant XX germ cells exhibit abnormally condensed  
370 chromosomes in ovaries and fail to undergo oogenesis after diplotene, showing that the sexual  
371 fate of XX germ cells turns into spermatogenesis (Kikuchi *et al.*, 2020). Thus, *fbxo47* is  
372 involved in the regulation of cell division in ovaies, and in turn the suppression of  
373 spermatogenesis in female germ cells in medaka. The germline feminization under *fbxo47* is  
374 mediated at least by two downstream transcription factors *lhx8b* and *figla* during early meiotic  
375 prophase in medaka. Despite the phenotypical similarities and differences observed in the  
376 mutants of Fbxo47 homologs in diverse organisms, FBXO47 homologs commonly act during  
377 meiotic prophase, although at different time points.

378

### 379 **Distinct interpretations on the function of FBXO47 in mouse**

380 Previous study showed that mouse FBXO47 interacts with SKP1 and telomere binding proteins,  
381 TRF1 and TRF2 (Hua *et al.*, 2019). According to the study, FBXO47 was localized to telomeres  
382 during meiotic prophase. Furthermore, TRF2 were destabilized and telomeres were detached  
383 from the nuclear envelope in *Fbxo47* KO spermatocytes, causing defects in telomere bouquet  
384 formation (Hua *et al.*, 2019). Those observations led to propose that FBXO47 binds to telomeric  
385 proteins TRF1 and TRF2, and plays a role in protecting TRF2 from destruction (Hua *et al.*,  
386 2019). However, we failed to detect either TRF1 or TRF2 in FBXO47 immunoprecipitates from  
387 testis chromatin fraction (Fig. S3A). Further, we failed to observe localization of FBXO47 to  
388 telomeres (Fig. S3B) and detachment of telomeres from nuclear envelope in *Fbxo47* KO  
389 spermatocytes (Fig. S3C), which contrast to the previous report (Hua *et al.*, 2019). Since the  
390 frequency of bouquet formation was quite low even in WT spermatocytes in mouse (Fig. S3D),  
391 as shown in our previous study (Ishiguro *et al.*, 2014), the potential defect in bouquet formation  
392 in *Fbxo47* KO spermatocytes further needs to be evaluated. Furthermore, our SKP1  
393 immunoprecipitation from *Skp1-3xFLAG-HA* KI testes (Fig. 2D, Supplementary Data1) and  
394 reciprocal FBXO47 immunoprecipitation from *Fbxo47-3xFLAG-HA* KI testes (Fig. 1H, Fig S2)  
395 failed to show supporting evidence that FBXO47 serves as a subunit of SCF. Although we do  
396 not know the exact reason for the discrepancies between the two studies with similar histological  
397 phenotype of the seminiferous tubules in *Fbxo47* KO testes, subtle differences in the dection  
398 and assay conditions or mice that were used could account for the differences in the  
399 observations.

400

### 401 **Distant F-box proteins are involved in homolog synapsis**

402 SCF and F-box proteins are involved in the process of homolog synapsis during meiotic  
403 prophase in diverse organisms. In plants, although no *Fbxo47* homolog exsist, distant F-box  
404 proteins are involved in homolog synapsis. In rice plant (*Oryza sativa*), MEIOTIC F-BOX

405 (MOF) encodes a F-BOX protein, and interacts with OSK1, a homolog of SKP1 (He *et al.*,  
406 2016). MOF acts as a subunit of SCF and localizes on the chromosome during meiotic prophase.  
407 In *mof* mutant male meiocytes, telomeres were not clustered and homolog synapsis was lost as  
408 indicated by complete absence of ZEP1, a transverse filament of SC. Thus, MOF plays a role in  
409 telomere bouquet formation during homolog pairing in male meiocyte. In rice plant,  
410 ZYGOTENE1 (ZYG1) encodes another F-box protein that has a limited similarity to mouse  
411 FBL12 (Zhang *et al.*, 2017). In *zyg1* mutant, polarized enrichment of OsSAD1, a SUN-domain  
412 containing protein, along nuclear envelope was lost and full-length homolog pairing was  
413 consequently impaired. This led to defective DSB repair of meiotic recombination, causing both  
414 male and female sterility in *zyg1* mutant. Thus, ZYG1 also plays a role in telomere bouquet  
415 formation during homolog pairing in rice plant. These studies suggest that rice F-box proteins  
416 MOF and ZYG1 act as a SCF component, and play a role in bouquet formation rather than in  
417 the process of SC formation, which is different to the role of mouse FBXO47 in SC  
418 maintenance.

419  
420 In budding yeast, a F-box protein Cdc4 acts as a substrate subunit of SCF during meiotic  
421 prophase. SCF<sup>Cdc4</sup> is assumed to regulate SC assembly by counteracting the Pch2 (TRIP13 in  
422 mammals)-dependent negative action that induces SC disassembly (Zhu *et al.*, 2021). It is  
423 proposed that SCF<sup>Cdc4</sup> targets the putative negative regulator of SC assembly toward  
424 degradation, and in turn stabilizes SC. Although how Pch2 itself or its downstream factors is  
425 counteracted by SCF<sup>CDC4</sup> remains elusive, F-box protein Cdc4 acts for the maintenance of SC in  
426 budding yeast.

427 In *Drosophila* female, knockdown of *SkpA*, a *skp1* homolog, caused premature disassembly of  
428 SC (Barbosa *et al.*, 2021). Depletion of F-box proteins, *Fbxo42* and *Slmb/βTrcp*, showed  
429 incomplete formation and precocious disassembly of SC, which was similar to the observation  
430 in *Fbxo47* KO mouse. PP2A catalytic (C) subunit and structural (A) subunit were identified as a  
431 candidate substrate of *Fbxo42*. Since overexpression of a PP2A subunit *Wrd* (B56) phenocopied  
432 *Fbxo42* knockdown, the SCF<sup>Fbxo42</sup> is assumed to stabilize SC by restricting PP2A-*Wrd* (B56)  
433 association. In these regards, *Drosophila* *Fbxo42* and budding yeast *Cdc4* share a similar role to  
434 mouse *FBXO47* in maintaining SC stability.

435 Previous studies showed PLK1 mediated-phosphorylation regulate SC disassembly in mouse  
436 (Jordan *et al.*, 2012), and PP2A phosphatase inhibitor OA promotes premature exit from  
437 pachytene and SC disassembly (Cobb *et al.*, 1999). Thus, phosphorylation level of SC regulates  
438 its stability during meiotic cell cycle. Given that *FBXO47* exists in the cytosol rather than  
439 localizing to the chromatin (Fig. 1H), it is possible that *FBXO47* may protect the SC directly or  
440 indirectly from a putative destabilizer that regulates the phosphorylation level of SC during  
441 early meiotic prophase (Fig. 7). It is still a large enigma how *FBXO47* acts for preventing  
442 premature SC disassembly, and further investigation is required for understanding the precise  
443 mechanism of *FBXO47* function.

444  
445

446 **Acknowledgments**

447 The authors thank Kaho Okamura (Kumamoto University) for technical support, and Marry  
448 Ann Handel for provision of H1t antibody. This work was supported in part by KAKENHI  
449 grant (#21K15018 to N.T.), KAKENHI grant (#19K06642 to Y.T.), KAKENHI grant  
450 (#20K22638 to R.S.), and KAKENHI grants (#19H05743, #20H03265, #20K21504, #JP  
451 16H06276 to K.I.) from MEXT Japan; Grant from AMED PRIME (21gm6310021h0001 to  
452 K.I.). Grants from The Sumitomo Foundation; The Naito Foundation, Astellas Foundation for  
453 Research on Metabolic Disorders; Daiichi Sankyo Foundation of Life Science; The Uehara  
454 Memorial Foundation; The NOVARTIS Foundation (Japan) for the promotion of Science;  
455 Takeda Science Foundation (to K.I.).

456

457 **Author contributions:** N.Tanno, K.T. performed the cytological and biochemical analyses. R.S.  
458 performed reanalysis of scRNA-seq data. N.Tani performed MS analyses. Y.T.H. performed the  
459 RT-PCR. K.A. designed the knockout mice. S.F. performed histological analyses. N.Takeda  
460 assisted oocyte experiments. K.I. supervised experiments, conducted the study and wrote the  
461 manuscript.

462

463 **Declaration of interests:** The authors declare no competing interests.

464

465

466 **Figure legend**

467 **Figure 1. Identification of the meiosis-specific factor FBXO47**

468 (A) Genomic view of MEIOSIN binding peak over *Fbxo47* loci. Genomic coordinates were  
469 obtained from Ensembl.

470 (B) The expression of *Fbxo47* in WT and *Meiosin* KO was examined using RT-PCR. Testis  
471 RNA was obtained from WT (3 animals each for P8 and P10) and *Meiosin* KO (3 animals). The  
472 graph shows the expression level of *Fbxo47* normalized by that of *GAPDH* with SD. Expression  
473 level of *Fbxo47* in P10 WT was set to 1. Statistical significance is shown by *p*-value  
474 (Two-tailed t-test). \*:  $p < 0.05$ .

475 (C) The tissue-specific expression pattern of *Fbxo47* was examined by RT-PCR. Testis RNA  
476 was obtained from embryonic day 18 (E18), 3-weeks old (3w) and 8-weeks old (8w) male mice.  
477 Ovary RNA was obtained from adult 8-weeks old (8w) female mice. RT- indicates control PCR  
478 without reverse transcription.

479 (D) Expression patterns of *Fbxo47* and other key developmental genes are reanalyzed using  
480 public scRNA-seq data of spermatogenic cells in adult mouse testis (GEO: GSE109033)  
481 (Hermann *et al.*, 2018). Expression patterns of *Fbxo47* and other key developmental genes are  
482 shown in UMAP plots. Key developmental genes include *Zbtb16*: spermatogonia, *Stra8*:  
483 differentiating spermatogonia and pleleptotene spermatocyte, *Dmc1*: meiotic prophase  
484 spermatocyte, *Acrv1*: round and elongated spermatid. UMAP of *Zbtb16* and *Stra8* was adopted  
485 from our previous study (Horisawa-Takada *et al.*, 2021).

486 (E) Expression profiles of *Fbxo47*, *Stra8* and *Dmc1* in E11.5, E12.5, E13.5, E15.5 fetal ovaries  
487 along pseudotime trajectory of germ cells. Pseudotime analysis was performed by reanalyzing  
488 scRNA-seq data (DRA011172) (Shimada *et al.*, 2021). Pseudotime expression profile of *Stra8*  
489 was adopted from our previous study (Horisawa-Takada *et al.*, 2021).

490 (F) The expression pattern of *Fbxo47* in the embryonic ovary was examined by  
491 RT-qPCR. Average values normalized to E12.5 gonad are shown with SD from  
492 technical triplicates or quadruplicates. N=1 gonadal sample for each embryo.

493 (G) Schematic illustrations of the *Fbxo47-3xFLAG-HA* knock-in (*Fbxo47-3FH* KI) allele. Blue  
494 boxes represent exons. The stop codon in the exon 11 was replaced with in-frame *3xFLAG-HA*  
495 and the endogenous 3'UTR.

496 (H) Western blot showed immunoprecipitates after tandem affinity purifications using  
497 anti-FLAG and anti-HA from cytoplasmic and chromatin extracts of WT (non-tagged control)  
498 and *Fbxo47-3FH* KI mouse testes (P15-18). The same membrane was sequentially reblotted  
499 with different antibodies against the endogenous FBXO47 that we generated. rabbit M: rabbit  
500 anti-FBXO47 middle region, rabbit C: rabbit anti-FBXO47 C-terminal region, G.pig C: guinea  
501 pig anti-FBXO47 C-terminal region.

502

503 **Figure 2. FBXO47 is not involved in the function of SCF.**

504 (A) Schematic illustrations of the *Skp1-3xFLAG-HA* knock-in (*Skp1-3FH* KI) allele. Blue boxes  
505 represent exons. The stop codon in the exon 6 was replaced with in-frame *3xFLAG-HA* and the  
506 endogenous 3'UTR.

507 (B) Chromosome spreads of WT (non-tagged) and *Skp1-3FH* KI spermatocytes were  
508 immunostained as indicated. Scale bar: 5  $\mu$ m.

509 (C) Silver staining of the immunoprecipitates from cytosolic extracts of WT (non-tagged  
510 control) and *Skp1-3FH* KI mouse testes after tandem affinity purifications using anti-FLAG and  
511 anti-HA antibodies. Arrowhead: SKP1-3xFLAG-HA.

512 (D) The immunoprecipitates from the cytosolic fraction of the WT (non-tagged control) and  
513 *Skp1-3FH* KI testis extracts were subjected to liquid chromatography tandem-mass  
514 spectrometry (LC-MS/MS) analyses. The F-box-containing proteins and SCF subunits identified  
515 by the LC-MS/MS analysis are presented after excluding the proteins detected in the control  
516 mock purification. The proteins are listed with SwissProt accession number, the number of  
517 peptide hits and Mascot scores. Full list of identified proteins are shown in the Supplementary  
518 Data1. It is worth noting that SC central element components, Six6OS1 and SYCE1, were  
519 included in the LC-MS/MS data of SKP1-3xFLAG-HA immunoprecipitates (Supplementary  
520 Data1). This suggests that SCF E3 ubiquitin ligase may target those SC components using an  
521 F-box protein listed in the LC-MS/MS data as a substrate recognition subunit.

522 (E) Western blot showed immunoprecipitates from cytosolic extracts of WT (non-tagged  
523 control), *Fbxo47-3FH* KI and *Skp1-3FH* KI (heterozygous) testes after tandem affinity  
524 purifications using anti-FLAG and anti-HA antibodies. The same membrane was sequentially  
525 reblotted with different antibodies as indicated. Red \*: FBXO47-3xFLAG-HA, Green \*:

526 SKP1-3xFLAG-HA, Blue \*: endogenous SKP1, Black \*: non-specific band. Note that SKP1  
527 was not detected in FBXO47 immunoprecipitate from *Fbxo47-3FH* KI testis extracts, and  
528 reciprocally FBXO47 was not detected in SKP1 immunoprecipitate from *Skp1-3FH* KI testis  
529 extracts.

530 (F) Chromosome spreads of WT and *Fbxo47* KO spermatocytes were immunostained as  
531 indicated. Scale bar: 5  $\mu$ m.

532

### 533 **Figure 3. FBXO47 was expressed in early meiotic prophase**

534 (A) Testis sections from *Fbxo47-3FH* KI and control (non-tagged) mice (P15) were stained for  
535 HA, SYCP3 and DAPI. Average 21% of the seminiferous tubules that have SYCP3+  
536 spermatocytes showed HA+/SYCP3+ in *Fbxo47-3FH* KI testes (n = 3 animals), while none of  
537 those was HA+/SYCP3+ in WT (n = 3 animals). Scale bar: 100  $\mu$ m.

538 (B) Seminiferous tubule sections from *Fbxo47-3FH* KI and control (non-tagged) mice (P15)  
539 were stained for HA, SYCP3,  $\gamma$ H2AX and DAPI. Lep: leptotene. Scale bar: 25  $\mu$ m.

540 (C) Seminiferous tubule sections were stained for HA, SYCP3, SYCP1 and DAPI as in (B).  
541 Zyg: zygotene, Pac: pachytene spermatocyte, rS: round spermatid, eS: elongating spermatid.  
542 Scale bar: 25  $\mu$ m.

543 (D) Testis sections from *Fbxo47-3FH* KI and control (non-tagged) mice (n = 3 for each  
544 genotype, P18) were stained for HA, H1t and DAPI as in (A). Number of seminiferous tubules  
545 that have HA+/ H1t+ cells was counted per the seminiferous tubules that have H1t+  
546 spermatocyte cells (52, 36, 18 tubules for non-tagged control; 15, 51, 36 tubules for  
547 *Fbxo47-3FH* KI mice). Scale bar: 100  $\mu$ m.

548 (E) Seminiferous tubule sections (P18) were stained for HA, SYCP3, H1t and DAPI as in (B).  
549 Lep: leptotene, Pac: pachytene spermatocyte, rS: round spermatid, eS: elongating spermatid.  
550 Scale bar: 25  $\mu$ m.

551 (F) Seminiferous tubule sections (8-weeks old) were immunostained as in (E). Lep: leptotene,  
552 Pac: pachytene spermatocyte, eS: elongating spermatid. Scale bar: 25  $\mu$ m. Note that pachy  
553 signals of HA immunostaining were nonspecific, since they were visible in control.

554

### 555 **Figure 4. Spermatogenesis was impaired in *Fbxo47* knockout male**

556 (A) The allele with targeted deletion of Exon3-13 in *Fbxo47* gene was generated by the  
557 introduction of CAS9, the synthetic gRNAs designed to target intron2 and the downstream of  
558 Exon11 (arrowheads), and ssODN (green and red boxes) into C57BL/6 fertilized eggs.

559 (B) *Fbxo47* mRNA expression was examined by RT-PCR. Testis RNA was obtained from  
560 *Fbxo47*+/- and *Fbxo47* KO males (P13). RT- indicates control PCR without reverse  
561 transcription.

562 (C) Testes from *Fbxo47*+/- and *Fbxo47* KO (8-weeks old). Testis/body-weight ratio (mg/g) of  
563 *Fbxo47*+/- and *Fbxo47* KO mice (8-weeks old) is shown on the right (Mean with SD). n: the  
564 number of animals examined. Statistical significance is shown by \*\*\*\*:  $p < 0.0001$  (Two-tailed  
565 t-test). Scale bar: 5 mm.

566 (D) Hematoxylin and eosin staining of the sections from *Fbxo47*<sup>+/-</sup> and *Fbxo47* KO testes  
567 (8-weeks old). Biologically independent mice for each genotype were examined. Scale bar: 100  
568  $\mu\text{m}$ .  
569 (E) Hematoxylin and eosin staining of the sections from *Fbxo47*<sup>+/-</sup> and *Fbxo47* KO epididymis  
570 (8-weeks old). Biologically independent mice for each genotype were examined. Scale bar: 100  
571  $\mu\text{m}$ .  
572 (F) Seminiferous tubule sections (8-weeks old) were stained for SYCP3, PNA lectin and DAPI.  
573 Note that the seminiferous tubule that contained PNA-positive elongated spermatids were not  
574 identified in *Fbxo47* KO testes. Scale bar: 25  $\mu\text{m}$ .  
575 (G) Number of pups born by mating *Fbxo47*<sup>+/-</sup> and *Fbxo47* KO males with *Fbxo47*<sup>+/-</sup> or  
576 *Fbxo47* KO females (N = number of females in the same cage) to examine fertility. *Fbxo47* KO  
577 male #1 was initially mated with three *Fbxo47*<sup>+/-</sup> females (all 6-weeks old at the start point of  
578 mating). After one month, another *Fbxo47* KO male #2 was started to cohabit with those  
579 females (8-weeks old at the start point of mating). This cage was observed for 3 months from  
580 the start of mating.  
581 (H) Hematoxylin and Eosin stained sections of *Fbxo47*<sup>+/-</sup> and *Fbxo47* KO ovaries (8-weeks  
582 old). Scale bar: 100 $\mu\text{m}$ .  
583 (I) Giemza staining of metaphase I chromosomes from *Fbxo47*<sup>+/-</sup> (N=20) and *Fbxo47* KO  
584 spermatocytes (N=26).  
585 (J) Cumulative number of pups born from *Fbxo47*<sup>+/-</sup> (n=4, all 6-weeks old at the start point of  
586 mating) and *Fbxo47* KO (n=4, all 6-weeks old at the start point of mating) females.  
587

588 **Figure 5. Premature disassembly of SC in *Fbxo47* KO spermatocytes.**

589 (A) Seminiferous tubule sections (P18 and 8-weeks old) were stained for SYCP3, H1t and  
590 DAPI. Pa: pachytene spermatocyte, rS: round spermatid, eS: elongating spermatid. Shown on  
591 the right is the quantification of the seminiferous tubules that have H1t<sup>+</sup>/SYCP3<sup>+</sup> cells per the  
592 seminiferous tubules that have SYCP3<sup>+</sup> spermatocyte cells in WT and *Fbxo47* KO mice (Mean  
593 with SD). n: the number of animals examined for each genotype. Statistical significance is  
594 shown (Unpaired t-test). \*\* :  $p = 0.0012$  for *Fbxo47* heterozygous versus *Fbxo47* KO at P18.  
595 *Fbxo47* heterozygous (p18: 62, 61, 29 tubules/animal were counted from 3 animals; 8w: 135,  
596 143, 45 tubules/animal were counted from 3 animals) and *Fbxo47* KO testes (p18: 105, 59,  
597 141 tubules/animal were counted from 3 animals; 8w: 36, 55, 63, 64, 88, 69, 108  
598 tubules/animal were counted from 7 animals). Scale bar: 25  $\mu\text{m}$ .  
599 (B) Chromosome spreads of WT and *Fbxo47* KO spermatocytes (3-4 weeks old) were  
600 immunostained as indicated. Enlarged images are shown to highlight de-synapsed chromosomes  
601 in diplotene-like *Fbxo47* KO spermatocytes. Scale bar: 5  $\mu\text{m}$ .  
602 (C) Quantification of meiotic prophase stage spermatocytes per total SYCP3<sup>+</sup> spermatocytes in  
603 WT and *Fbxo47* KO mice at P15 and P18 is shown. n: the number of cells examined.  
604 (D) Chromosome spreads of pachytene and diplotene-like *Fbxo47* KO spermatocyte were  
605 immunostained for SYCP3, H3S10P and HORMAD1. Scale bar: 5  $\mu\text{m}$ .

606 (E) Chromosome spreads of diplotene spermatocyte in the control and diplotene-like  
607 spermatocyte in *Fbxo47* KO spermatocytes (P18) were immunostained for SYCP3, H3S10P and  
608 DAPI. Scale bar: 5  $\mu$ m. Note that centromeric regions are positively stained for H3S10P in the  
609 control diplotene spermatocyte but not in diplotene-like spermatocyte in *Fbxo47* KO  
610 spermatocytes.  
611 (F) Spermatocytes isolated from the control *Fbxo47*<sup>+/-</sup> and *Fbxo47* KO testes were cultured *in*  
612 *vitro* in the presence or absence of OA for 3 hours. Quantification of meiotic prophase stage is  
613 shown on the right. n: the number of cells examined. Note that the control spermatocytes  
614 showed a typical feature of diakinesis/Meta I with condensed chromosomes and remaining  
615 SYCP3 at centromeres.  
616 (G) Seminiferous tubule sections from 8-weeks old mice were subjected to TUNEL assay with  
617 immunostaining for SYCP3. L: leptotene, Pa: pachytene. Shown on the right is the  
618 quantification of the seminiferous tubules that have TUNEL<sup>+</sup> cells per total tubules in  
619 *Fbxo47*<sup>+/-</sup> (8w; n=3) and *Fbxo47* KO (8w; n=3) testes (mean with SD). Statistical significance  
620 is shown by \*\*  $p = 0.0072$  (Two-tailed t-test). Scale bar: 25  $\mu$ m.  
621 (H) Schematic illustration of the precocious SC disassembly observed in *Fbxo47* KO  
622 spermatocytes. The expression timing of H1t and H3S10P markers is shown.  
623

624 **Figure 6. *Fbxo47* KO spermatocytes show defects in meiotic recombination**

625 (A) Chromosome spreads of WT and *Fbxo47* KO spermatocytes were immunostained for  
626 SYCP3, SYCP1 and  $\gamma$ H2AX.  
627 (B) Chromosome spreads of WT and *Fbxo47* KO spermatocytes were immunostained for  
628 SYCP3, SYCP1 and BRCA1.  
629 (C) Chromosome spreads of WT and *Fbxo47* KO spermatocytes were stained as indicated.  
630 Immunostained chromosome spread of pachytene spermatocytes are shown.  
631 The number of RAD51 foci is shown in the scatter plot with median (right). Statistical  
632 significance is shown by  $p$ -value (Mann-Whitney U-test). \*\*\*\*:  $p < 0.0001$ . \*\*\*:  $p < 0.001$ . \*\*:  
633  $p < 0.01$ . Lep.: leptotene, Zyg.: Zygotene, Pac.: Pachytene, Z-like: Zygotene-like, P-like:  
634 Pachytene-like, D-like: Diplotene-like. n: the number of cells examined.  
635 (D) Chromosome spreads of WT and *Fbxo47* KO spermatocytes were stained as indicated. The  
636 number of MSH4 foci is shown in the scatter plot with median (right). Statistical significance is  
637 shown by  $p$ -value (Mann-Whitney U-test). \*:  $p < 0.05$ .  
638 (E) Chromosome spreads of *Fbxo47*<sup>+/-</sup> and *Fbxo47* KO spermatocytes were stained as  
639 indicated. The number of MLH1 foci is shown in the scatter plot with median (right). Statistical  
640 significance is shown by  $p$ -value (Mann-Whitney U-test). \*\*\*:  $p < 0.0001$ . Scale bars: 5  $\mu$ m.  
641

642 **Figure 7. A model of FBXO47 function to prevent premature SC disassembly**

643 Schematic illustration how FBXO47 may protect SC from a putative destabilizer during early  
644 meiotic prophase.  
645

646 **Supplementary Figure 1. Generation of *Fbxo47-3xFLAG-HA* knock-in mice**



647 (A) Testes from WT (no-tagged) and the *Fbxo47-3xFLAG-HA* KI homozygous mice (8-weeks  
648 old). Scale bar: 5 mm.

649 (B) Hematoxylin and eosin staining of the testes (upper) and epididymis (lower) sections from  
650 WT (non-tagged control) and the *Fbxo47-3xFLAG-HA* KI homozygous testes (8-weeks old).  
651 Scale bar: 100  $\mu$ m.

652 Note that The FBOX47-3xFLAG-HA fusion protein was physiologically functional considering  
653 the normal fertility shown in homozygous male and female mice with the KI allele.

654

#### 655 **Supplementary Figure 2. MS analyses of FBXO47 interacting factors in testis extracts**

656 The immunoprecipitates (IP) from the cytosolic fraction of the testis extracts were subjected to  
657 liquid chromatography tandem-mass spectrometry (LC-MS/MS) analyses. The proteins  
658 identified by the LC-MS/MS analysis of FBXO47-IP are presented after excluding the proteins  
659 detected in the control IgG-IP. The proteins with more than 1 different peptide hits are listed  
660 with UniProt accession number, the number of peptide hits and Mascot scores.

661

#### 662 **Supplementary Figure 3. FBXO47 do not localize to telomeres**

663 (A) Western blot showed immunoprecipitates from chromatin extracts of WT (non-tagged  
664 control) and *Fbxo47-3FH* KI mouse testes (from 139 and 148 animals at P14-19, respectively)  
665 after tandem affinity purifications using anti-FLAG and anti-HA antibodies. The same  
666 membrane was sequentially reblotted with different antibodies as indicated. \*: non-specific  
667 band. Arrowhead: TRF2. Note that western blot did not detecte either TRF1 or TRF2 in the  
668 FBXO47 immunoprecipitate.

669 (B) Chromosome spreads of *Fbxo47-3FH* KI and control (non-tagged) spermatocytes were  
670 immunostained as indicated. Images with enhanced contrast for HA color channel are shown.  
671 Scale bar: 5  $\mu$ m. Note that FBXO47 did not show specific localization pattern to telomeres. We  
672 observed no more than background signals, even though contrast for HA images was enhanced.

673 (C) Structurally-preserved nuclei of spermatocytes were prepared by squashing *Fbxo47* KO  
674 testis tubules, and immunostained for LAMIN-B, TRF1 and SYCP3. The image acquired at the  
675 equator of the spermatocyte nuclei is shown. Note that telomeres attachment to the nuclear  
676 envelope was intact in *Fbxo47* KO spermatocytes.

677 (D) The indicated spermatocyte nuclei were immunostained as indicated (Upper). Telomere  
678 clustering in wild-type (n=355) and *Fbxo47* KO (n=342) was scored at 12 day post-partum. The  
679 frequency of bouquet stage spermatocytes is shown (Bottom). Statistical significance is shown  
680 by N.S.  $p = 0.5025$  (chi square-test).

681

#### 682 **Supplementary Figure 4. Uncropped images of gels and blots**

683 Full-length / uncropped images of agarose gel (Fig1C, Fig4B) and immunoblots (Fig1H, Fig2E,  
684 Fig S3A) are shown. Immunoblotted membrane was sequentially reprobed with different  
685 antibodies. For SKP1, H3, TRF1 immunoblots, the same membrane was stripped, cut according  
686 to molecular weight marker and reprobed with different antibody, so that different proteins

687 could be simultaneously probed with different antibodies. For Fig2E, the membrane was first  
688 immunoblotted with anti-HA antibody. After stripping, immunoblotted membrane was cut at a  
689 height of between 37 kDa and 25 kDa. Upper and lower membrane was immunoblotted with  
690 rabbit anti-FBXO47 middle region antibody and rabbit anti-SKP1 antibody, respectively. The  
691 membrane was combined and images were acquired sequentially at different exposure time.

692

693

694 **Supplementary Data1 (Excel). Whole list of identified proteins by MS analyses of FBXO47**  
695 **IP and SKP1 IP from testis extracts**

696 Coloidal blue stained gel after running the samples is shown in the first tab. Gel was cut into  
697 pieces before LC-MS/MS analysis. Full list of proteins identified by the LC-MS/MS analysis  
698 are shown in the second tab. The proteins are listed with UniProt accession number, the number  
699 of peptide hits and Mascot scores. In the third tab, proteins are presented after excluding the  
700 proteins detected in the control mock purification, IgG and keratin.

701

702 **Supplementary Data2 (Excel). The source data for statistics**

703 The source data (for Fig.1B, Fig.1F, Fig.4C, Fig.4G, Fig. 4I, Fig. 4J, Fig. 5A, Fig. 5C, Fig. 5F,  
704 Fig.5G, Fig. 6C, Fig. 6D, Fig. 6E) are shown in the tabs.

705

706

707 **STAR Methods**

708 **Lead Contact and Material Availability**

709 Further information and requests for the resources and reagents should be directed to and will be  
710 fulfilled by the Lead Contact, Kei-ichiro Ishiguro ([ishiguro@kumamoto-u.ac.jp](mailto:ishiguro@kumamoto-u.ac.jp)).

711 All data supporting the conclusions are present in the paper and the supplementary materials.

712 The source data (for Fig.1B, Fig.1F, Fig.4C, Fig.4G, Fig. 4I, Fig. 4J, Fig. 5A, Fig. 5C, Fig. 5F,  
713 Fig.5G, Fig. 6C, Fig. 6D, Fig. 6E, FigS3D) are provided in Supplementary data2 (Excel). The

714 original images for all of the figures in this paper are deposited in public depository.

715 The CHIP-seq data of MEIOSIN and STRA8 are described in our previous study (Ishiguro *et al.*,

716 2020) and available in the DDBJ Sequence Read Archive (DRA) under accession number

717 DRA007066, DRA007778, DRA009056. Mouse lines generated in this study have been

718 deposited to Center for Animal Resources and Development (CARD), *Fbxo47* Ex3-11Δ

719 knockout mouse (ID 2777), *Fbxo47-3xFLAG-HA* knock-in mouse (ID 2972), and

720 *Skp1-3xFLAG-HA* knock-in mouse (ID 2638). Plasmid expression vectors generated in this

721 study have been deposited to RIKEN BRC: pET28c-*Fbxo47*-C (aa272-451) (ID RDB192639)

722 and pET28c-*Fbxo47*-M (aa174 -316) (ID RDB19264). The antibodies are available upon

723 request. There are restrictions to the availability of antibodies due to the lack of an external

724 centralized repository for their distribution and our need to maintain the stock. We are glad to

725 share antibodies with reasonable compensation by the requestor for its processing and shipping.

726 All unique/stable reagents generated in this study are available from the Lead Contact with a

727 completed Materials Transfer Agreement.

728

## 729 **Experimental Model and Subject Details**

### 730 **Animals**

731 *Fbxo47* Ex3-11Δ knockout and *Fbxo47-3xFLAG-HA* knock-in mice were C57BL/6 background.  
732 *Skp1-3xFLAG-HA* knock-in mouse was congenic with C57BL/6 background. Male mice were  
733 used for immunoprecipitation of testis extracts, histological analysis of testes, immunostaining  
734 of testes, and RT-PCR experiments. Female mice were used for histological analysis of the  
735 ovaries, and immunostaining experiments. Whenever possible, each knockout animal was  
736 compared to littermates or age-matched non-littermates from the same colony, unless otherwise  
737 described. Animal experiments were approved by the Institutional Animal Care and Use  
738 Committee (approval F28-078, A30-001, A28-026, A2020-006).  
739

### 740 **Method Details**

#### 741 **Generation of *Fbxo47* knockout mice and genotyping**

742 *Fbxo47* knockout mouse was generated by introducing Cas9 protein (317-08441; NIPPON  
743 GENE, Toyama, Japan), tracrRNA (GE-002; FASMAC, Kanagawa, Japan), synthetic crRNA  
744 (FASMAC), and ssODN into C57BL/6N fertilized eggs using electroporation. For generating  
745 *Fbxo47* Exon3-11 deletion (Ex3-11Δ) allele, the synthetic crRNAs were designed to direct  
746 TACACCTAGTGATAGCACTT(GGG) of the *Fbxo47* intron 2 and  
747 AGAGCACTAGTCACTGAATG(CGG) in the 3'-neighboring region of the Exon11. ssODN:  
748 5'-  
749 GCTCAAAGTAAGCAAAGCAACAGAGAGCACTAGTCACTGATTATTTATTCAGTTGG  
750 GATGCTGAGGAGGCAAATTGCCAGGTGTTTGAAGC  
751 -3' was used as a homologous recombination template.  
752 The electroporation solutions contained (10μM of tracrRNA, 10μM of synthetic crRNA, 0.1  
753 μg/μl of Cas9 protein, 1μg/μl of ssODN) for *Fbxo47* knockout in Opti-MEM I Reduced Serum  
754 Medium (31985062; Thermo Fisher Scientific). Electroporation was carried out using the Super  
755 Electroporator NEPA 21 (NEPA GENE, Chiba, Japan) on Glass Microslides with round wire  
756 electrodes, 1.0 mm gap (45-0104; BTX, Holliston, MA). Four steps of square pulses were  
757 applied (1, three times of 3 mS poring pulses with 97 mS intervals at 30 V; 2, three times of 3  
758 mS polarity-changed poring pulses with 97 mS intervals at 30 V; 3, five times of 50 mS transfer  
759 pulses with 50 mS intervals at 4 V with 40% decay of voltage per each pulse; 4, five times of 50  
760 mS polarity-changed transfer pulses with 50 mS intervals at 4 V with 40% decay of voltage per  
761 each pulse).  
762 The targeted *Fbxo47* Ex3-11Δ allele in F0 mice were identified by PCR using the following  
763 primers:

764 Fbxo47-F1: 5'-TCCTCTCTCTGTCTCTTTATTCAACAG-3' and Fbxo47-R1: 5'-  
765 TGCTAAGAAGGTGGTAAAGAATGTGAC-3' for the knockout allele (825 bp). Fbxo47-F3:  
766 5'- TCTGACCATGAACGCTATCTCTTCC-3' and Fbxo47-R1 for wild-type allele (503 bp).  
767 The PCR amplicons were verified by sequencing. Primer sequences are listed in Table S1.  
768

#### 769 **Generation of *Fbxo47-3xFLAG-HA* knock-in mice and genotyping**

770 *Fbxo47-3xFLAG-HA* knock-in mouse was generated by introducing Cas9 protein, tracrRNA,  
771 synthetic crRNA, and ssODN into C57BL/6N fertilized eggs using electroporation as described  
772 above. The synthetic crRNA was designed to direct ACGCTATCTCTTCCTAAGTC(AGG) of  
773 the *Fbxo47*.

774 ssODN:

775 5'-GAACTTCCATAAGGAGGTGCTGTATCTGACCATGAACGCTATCTCTTCCGGAGAC  
776 TACAAAGACCATGACGGTGATTATAAAGATCATGACATCGATTACAAGGATGACGA  
777 TGACAAGGGATAACCCCTACGACGTGCCCGACTACGCCTAAGTCAGGAAGCTTGTGT  
778 CCCTCTGGACTGGCATTTCAGGGGAGTGATGCC-3'

779 was used as a homologous recombination template.

780 The targeted *Fbxo47-3xFLAG-HA* knock-in allele in F0 mice were identified by PCR using the  
781 following primers:

782 Fbxo47-F4: 5'-TCTGTTCCATCTTCTCCATGCTCAGGC-3' and Fbxo47-R3: 5'-  
783 TGAAGAGCCAGAACTTGTTTTCCAG-3' for the knock-in allele (396 bp), and for wild-type  
784 allele (294 bp). The PCR amplicons were verified by sequencing. Primer sequences are listed in  
785 Table S1.  
786

#### 787 **Generation of *Skp1-3xFLAG-HA* knock-in mouse and genotyping**

788 The targeting vector was designed to insert 3xFLAG-HA-3'UTR in frame with the coding  
789 sequence into the Exon 6 of the *Skp1* genomic locus. Targeting arms of 1225bp and 1481bp  
790 fragments, 5' and 3' of the Exon 6 of *Skp1* gene respectively, were generated by PCR from  
791 mouse C57BL/6 genomic DNA and directionally cloned flanking p*GK-Neo*-polyA and *DT-A*  
792 cassettes. The 5' arm was followed by nucleotide sequences encoding 3xFLAG, HA and the  
793 3'UTR of *Skp1* gene. TT2 ES cells were co-transfected with the targeting vector and pX330  
794 plasmids (Addgene) expressing Crispr-gRNAs directing GCTGGCATTGACTCGGGGTA(ggg)  
795 and CGCCACCATAACCCGGTGATT (tgg), which locate at the 3' region of the Exon 6 of *Skp1*  
796 gene. The G418-resistant ES clones were screened for homologous recombination with the *Skp1*  
797 locus by PCR using primers SKP1\_5Arm\_F2: 5'-

798 GGTCAGCAAACTGCTGAACAGCTTG-3' and

799 KI96ES-19814R-HA: 5'- GGGCACGTCGTAGGGGTATCCCTTG -3' for the left arm (1909  
800 bp); pKO2-3armF: 5'-AGGAACTTCGGAATAGGAAC-3' and

801 SKP1\_RightArm\_R2: 5'-TGCAGTGGAGGCTCAGTCCAGCTTC-3' for the right arm (1897  
802 bp).  
803

804 The homologous recombinant cells were isolated and chimeric mice were generated by  
805 aggregation (host ICR) of recombinant ES cells. Chimeric males were mated to C57BL/6N  
806 females and the progenies were genotyped by PCR using the primers:  
807 SKP1onL2\_F2: 5'- ATCATTGTTCCCAGGTGGAG -3' and  
808 SKP1onRight\_R1: 5'- GACTAGAACAAGATGACAGG -3'  
809 for the knock-in allele (2078 bp) and the WT allele (1275bp). Primer sequences are listed in  
810 Table S1.

811

### 812 **Histological Analysis**

813 Testes, caudal epididymis and ovaries were fixed in Bouin's solution, and embedded in paraffin.  
814 Sections were prepared on CREST-coated slides (Matsunami) at 6 µm thickness. The slides  
815 were deparaffinized and stained with hematoxylin and eosin.  
816 For Immunofluorescence staining, testes were embedded in Tissue-Tek O.C.T. compound  
817 (Sakura Finetek) and frozen. Cryosections were prepared on the CREST-coated slides  
818 (Matsunami) at 8 µm thickness, and then air-dried. The serial sections of frozen testes were  
819 fixed in 4% paraformaldehyde in PBS for 5 min at room temperature and washed briefly in PBS.  
820 After washing, the serial sections were permeabilized in 0.1% TritonX100 in PBS for 5 min.  
821 The sections were blocked in 3% BSA/PBS, and incubated at room temperature with the  
822 primary antibodies in a blocking solution. After three washes in PBS, the sections were  
823 incubated for 1 h at room temperature with Alexa-dye-conjugated secondary antibodies (1:1000;  
824 Invitrogen) in a blocking solution. PNA lectin staining was done using FITC-conjugated  
825 Lectin from *Arachis hypogaea* (IF, 1:1000, Sigma: L7381). TUNEL assay was performed  
826 using MEBSTAIN Apoptosis TUNEL Kit Direct (MBL 8445). DNA was counterstained with  
827 Vectashield mounting medium containing DAPI (Vector Laboratory).

828

### 829 **Immunostaining of spermatocytes**

830 Surface-spread nuclei from spermatocytes were prepared by the dry down method as described  
831 (Peters et al., 1997) (Takemoto et al., 2020) with modification. The slides were then air-dried  
832 and washed with water containing 0.1 % TritonX100 or frozen for longer storage at -30°C. The  
833 slides were permeabilized in 0.1% TritonX100 in PBS for 5 min, blocked in 3% BSA/PBS, and  
834 incubated at room temperature with the primary antibodies in 3% BSA/PBS. After three washes  
835 in PBS, the sections were incubated for 1 h at room temperature with Alexa-dye-conjugated  
836 secondary antibodies (1:1000; Invitrogen) in a blocking solution. For bouquet counting, cells  
837 were suspended in PBS without hypotonic treatment and structurally preserved nuclei of  
838 spermatocytes were prepared by cytopspin at 1000rpm for 5min (Thermofisher). Cells were fixed  
839 with 4% PFA in PBS for 5 min. The slide grasses were washed with PBS containing 0.1%  
840 Triton-X100 in PBS. After washing with PBS, immunofluorescence staining was performed  
841 immediately. DNA was counterstained with Vectashield mounting medium containing DAPI  
842 (Vector Laboratory).

843

### 844 **Imaging**

845 Immunostaining images were captured with DeltaVision (GE Healthcare). The projection of the  
846 images was processed with the SoftWorx software program version 7.2.1 (GE Healthcare). All  
847 images shown were Z-stacked. Bright field images and immunofluorescent images for counting  
848 seminiferous tubules, were captured with BIOREVO BZ-X710 (KEYENCE), and processed  
849 with BZ-H3A program. XY-stitching capture by 10x objective lens was performed for  
850 multiple-point color images using BZ-X Wide Image Viewer. Images were merged over the  
851 field using BZ-H3A Analyzer (KEYENCE). If the SYCP3 image was too dim for counting the  
852 SYCP3+ seminiferous tubules, the contrast of the color channel used for SYCP3 was enhanced  
853 in the XY-stitched image.

854

855

856

### 857 ***In vitro* oocyte culture and Giemsa staining of metaphase chromosome spread**

858 Ovaries collected from 4-week-old female mice were used after 46 to 48 h of treatment with 5  
859 IU of pregnant mare serum gonadotropin. GV oocytes were isolated by puncturing the follicles  
860 in M2 medium (Sigma MR-015). The GV oocytes were cultured in M16 medium (Sigma  
861 MR-016) in a 5% CO<sub>2</sub> atmosphere at 37°C for 6hours. For Giemsa staining of metaphase  
862 chromosome spread, oocytes were exposed to 0.5% Pronase (MERCK 10165921001) to remove  
863 the zona pellucida, and treated in hypotonic buffer containing 1% sodium citrate/0.1% PVA for  
864 15min. The oocytes and oocyte-like cells were placed on the slides, fixed in the Carnoy's  
865 Fixative (75 % Methanol, 25% Acetic Acid), and stained in 3% Giemsa solution for 30min.

866

### 867 **Culture of OA-induced Meta I spermatocyte**

868 Culture of OA-induced Meta I spermatocytes were performed as described (Wiltshire et al.,  
869 1995). The isolated spermatocytes were cultured in the presence or absence of 5 μM okadaic  
870 acid (OA) for 3 h.

871

### 872 **Antibodies**

873 The following antibodies were used for immunoblot (IB) and immunofluorescence (IF) studies:  
874 mouse anti-FLAG M2 (Sigma-Aldrich F1804), rabbit anti-HA (IB, IF, 1:1000, Abcam: ab91110),  
875 rabbit anti-Actin (IB, 1:1000, Sigma-Aldrich A2066), mouse anti-MLH1 (IF, 1:500, BD  
876 Biosciences: 551092), rabbit anti-H3S10p (IF, 1:2000, Abcam ab5176), rabbit anti-Histone H3  
877 (IB, 1:1000, Abcam ab1791), rabbit anti-SYCP1 (IF, 1:1000, Abcam ab15090), mouse  
878 anti-gH2AX (IF, 1:1000, Abcam ab26350), rabbit anti-RAD51 (IF, 1:500, Santa Cruz:  
879 SC-8349), rabbit anti-MSH4 (IF, 1:500, Abcam ab58666), rabbit anti-SKP1 (IB, 1:1000,  
880 Abcam ab10546), rabbit anti-HORMAD1 (IF, 1:1000, ProteinTech 13917-1-AP), goat  
881 anti-Lamin B (IF, 1:1000, Santa Cruz: SC-6216), mouse anti-TRF1 (Shibuya et al., 2014) (IF,  
882 1:1000), rabbit anti-TRF1 (Shibuya *et al.*, 2014) (IB, 1:1000), rabbit anti-TRF2 (IB, 1:1000,  
883 NB110-57130), mouse anti-SYCP1 (IF, 1:1000) (Ishiguro et al., 2011), rat anti-SYCP3  
884 (Ishiguro *et al.*, 2020) (IF, 1:1000), guinea pig anti-SYCP3 (Ishiguro *et al.*, 2020) (IF, 1:2000),

885 rabbit anti-BRCA1 (IF, 1:500, kindly provided by Satoshi Namekawa), guinea pig anti-H1t (IF,  
886 1:2000, kindly provided by Marry Ann Handel).

887

#### 888 **Production of antibodies against FBXO47**

889 Polyclonal antibodies against mouse FBXO47 C-terminal (aa272-451) were generated by  
890 immunizing rabbits and a guinea pig. FBXO47 middle region (aa174-316) were generated by  
891 immunizing a rabbit. His-tagged recombinant proteins of FBXO47 middle region (aa174-316)  
892 and C-terminal (aa272-451) were produced by inserting cDNA fragments in-frame with pET19b  
893 and pET28c (Novagen) respectively in *E. coli* strain BL21-CodonPlus (DE3)-RIPL (Agilent),  
894 solubilized in a denaturing buffer (6 M HCl-Guanidine, 20 mM Tris-HCl pH 7.5) and purified  
895 by Ni-NTA (QIAGEN) under denaturing conditions. The antibodies were affinity-purified from  
896 the immunized serum with immobilized antigen peptides on CNBr-activated Sepharose (GE  
897 healthcare).

898

#### 899 **PCR with reverse transcription.**

900 Total RNA was isolated from tissues and embryonic gonads using TRIzol (Thermo Fisher).  
901 cDNA was generated from total RNA using Superscript III (Thermo Fisher) followed by PCR  
902 amplification using Ex-Taq polymerase (Takara) and template cDNA.

903 For RT-qPCR, total RNA was isolated from WT (n = 3) and *Meiosin* KO (n = 3) testes, and  
904 cDNA was generated as described previously (Ishiguro *et al.*, 2020). *Fbxo47* cDNA was  
905 quantified by  $\Delta$ CT method using TB Green Premix Ex Taq II (Tli RNaseH Plus) and Thermal  
906 cycler Dice (Takara), and normalized by *GAPDH* expression level.

907 qPCR was performed in duplicates, and the average ddCt value was calculated for each cDNA  
908 sample. The expression level of *Fbxo47* was divided by that of *GAPDH* to give the relative  
909 expression level of *Fbxo47* to *GAPDH*. Relative expression level of *Fbxo47* to *GAPDH* was  
910 normalized to 1 for a given P10 WT sample.

911 Sequences of primers used for RT-PCR were as follows:

912 GAPDH-F: 5'-TTCACCACCATGGAGAAGGC-3'

913 GAPDH-R: 5'-GGCATGGACTGTGGTCATGA-3'

914 Gapdh\_F2: 5'-ACCACAGTCCATGCCATCAC-3'

915 Gapdh\_R2: 5'-TCCACCACCCTGTTGCTGTA-3'

916 Gapdh\_Ex6F: 5'-GGTTGTCTCCTGCGACTTCA-3'

917 Gapdh\_mRNAR: 5'-GCCGTATTCATTGTCATACCAGG-3'

918 *Fbxo47*-F 1443F: 5'-GCATAGCAAATGCTTTTGCCTGTG-3'

919 *Fbxo47*-R 1605R: 5'-GAGATAGCGTTCATGGTCAGATAC-3'

920 Primer sequences are listed in Table S1.

921

922

#### 923 **Preparation of testis extracts and immunoprecipitation**

924 Testis chromatin-bound and -unbound extracts were prepared as described previously (Ishiguro  
925 *et al.*, 2014). Briefly, testicular cells were suspended in low salt extraction buffer (20 mM

926 Tris-HCl pH 7.5, 100 mM KCl, 0.4 mM EDTA, 0.1% TritonX100, 10% glycerol, 1 mM  
927  $\beta$ -mercaptoethanol) supplemented with Complete Protease Inhibitor (Roche). After  
928 homogenization, the soluble chromatin-unbound fraction was separated after centrifugation at  
929 100,000g for 10 min at 4°C. The chromatin bound fraction was extracted from the insoluble  
930 pellet by high salt extraction buffer (20 mM HEPES-KOH pH 7.0, 400 mM KCl, 5 mM MgCl<sub>2</sub>,  
931 0.1% Tween20, 10% glycerol, 1 mM  $\beta$ -mercaptoethanol) supplemented with Complete Protease  
932 Inhibitor. The solubilized chromatin fraction was collected after centrifugation at 100,000g for  
933 10 min at 4°C.

934

### 935 **Immuno-affinity purification**

936 Immuno-affinity purification was performed with anti-FLAG M2 monoclonal antibody-coupled  
937 magnetic beads (Sigma-Aldrich M8823) from the testis chromatin-bound and -unbound  
938 fractions of *Fbxo47-3xFLAG-HA* knock-in mice and *Skp1-3xFLAG-HA* knock-in mice (14 to  
939 21-day old). For negative control, mock immuno-affinity purification was done from the testis  
940 chromatin-bound and -unbound fractions from the age-matched wild type mice. The beads were  
941 washed with high salt extraction buffer for chromatin-bound proteins and low salt extraction  
942 buffer for chromatin-unbound proteins. The anti-FLAG-bound proteins were eluted by 3xFLAG  
943 peptide (Sigma-Aldrich). The second immuno-affinity purification was performed anti-HA 5D8  
944 monoclonal antibody-coupled Magnet agarose (MBL M132-10). The bead-bound proteins were  
945 eluted with 40  $\mu$ l of elution buffer (100 mM Glycine-HCl pH 2.5, 150 mM NaCl), and then  
946 neutralized with 4  $\mu$ l of 1 M Tris-HCl pH 8.0.

947 The immunoprecipitated proteins were run on 4-12 % NuPAGE (Thermo-Fisher) in  
948 MOPS-SDS buffer and silver-stained with Silver Quest (Thermo-Fisher), immunoblotted or  
949 analyzed by LC-MS/MS. For the immunoblot of whole testes extracts from WT, *Fbxo47* KO,  
950 and *Fbxo47-3FH* KI mice, lysates were prepared in RIPA buffer and run on 8% Laemmli  
951 SDS-PAGE in Tris-Glycine-SDS buffer. Immunoblot images were developed using ECL prime  
952 (GE healthcare) and captured by FUSION Solo (VILBER).

953

### 954 **Mass spectrometry**

955 The immunoprecipitated proteins were run on 4-12 % NuPAGE (Thermo Fisher) by 1 cm from  
956 the well and stained with SimplyBlue (Thermo Fisher) for in-gel digestion. The gel containing  
957 proteins was excised, cut into approximately 1mm sized pieces. Proteins in the gel pieces were  
958 reduced with DTT (Thermo Fisher), alkylated with iodoacetamide (Thermo Fisher), and  
959 digested with trypsin and Lysyl endopeptidase (Promega) in a buffer containing 40 mM  
960 ammonium bicarbonate, pH 8.0, overnight at 37°C. The resultant peptides were analyzed on an  
961 Advance UHPLC system (ABRME1chrom Bioscience) connected to a Q Exactive mass  
962 spectrometer (Thermo Fisher) processing the raw mass spectrum using Xcalibur (Thermo Fisher  
963 Scientific). The raw LC-MS/MS data was analyzed against the NCBI non-redundant  
964 protein/translated nucleotide database restricted to *Mus musculus* using Proteome Discoverer  
965 version 1.4 (Thermo Fisher) with the Mascot search engine version 2.5 (Matrix Science). A  
966 decoy database comprised of either randomized or reversed sequences in the target database was



967 used for false discovery rate (FDR) estimation, and Percolator algorithm was used to evaluate  
968 false positives. Search results were filtered against 1% global FDR for high confidence level.  
969 All full lists of LC-MS/MS data are shown in Supplementary Data1 (Excel file).

970

971

#### 972 **ChIP-seq Data and Public RNA-seq data Analysis**

973 MEIOSIN ChIP-seq data described in our previous study (Ishiguro *et al.*, 2020) was analyzed  
974 for the *Fbxo47* locus. MEIOSIN binding site was shown along with genomic loci from Ensembl  
975 on the genome browser IGV.

976

#### 977 **Single cell RNA-seq Data Analysis**

978 The scRNA-seq data of fetal ovaries was derived from DRA 011172 (Shimada *et al.*, 2021).  
979 10xGenomics Drop-seq data of mouse adult testis was derived from GEO: GSE109033  
980 (Hermann *et al.*, 2018). Reanalyses of scRNA-seq data were conducted using the Seurat  
981 package for R (v.3.1.3) (Stuart *et al.*, 2019) and pseudotime analyses were conducted using  
982 monocle package for R: R (ver. 3.6.2), RStudio (ver.1.2.1335), and monocle (ver. 2.14.0) (Qiu  
983 *et al.*, 2017) following developer's tutorial.

984

#### 985 **Quantification and Statistical analysis**

986 Statistical analyses, and production of graphs and plots were done using GraphPad Prism8  
987 (version 8.4.3) or Microsoft Excel (version 16.48).

988

989 **Figure 1B** Testis RNA was obtained from P8 WT (3 animals), P10 WT (3 animals), *Meiosin*  
990 KO (3 animals). qPCR was performed in duplicates, and the average ddCt value was calculated  
991 for each cDNA sample. The expression level of *Fbxo47* was divided by that of *GAPDH* to give  
992 the relative expression level of *Fbxo47* to *GAPDH*. Relative expression level of *Fbxo47* to  
993 *GAPDH* was normalized to 1 for a given P10 WT sample. Bar graph indicates mean with SD.  
994 Statistical significance was determined by t-test.

995

996 **Figure 1F** RNA was obtained from WT Embryonic ovaries (E12.5 to E18.5). qPCR was  
997 performed in triplicates or quadruplicates, and the average ddCt value was calculated for each  
998 cDNA sample. The expression level of *Fbxo47* was divided by that of *GAPDH* to give the  
999 relative expression level of *Fbxo47* to *GAPDH*. Relative expression level of *Fbxo47* to *GAPDH*  
1000 was normalized to 1 for a given E12.5 WT sample. Bar graph indicates mean with SD.

1001

1002 **Figure 3A** Testis sections (P15) were obtained from non-tagged control (3 animals) and  
1003 *Fbxo47-3FH* KI (3 animals). Number of seminiferous tubules that have HA+/ SYCP3+ cells  
1004 was counted per the seminiferous tubules that have SYCP3+ spermatocyte cells (84, 85, 45  
1005 tubules for non-tagged control, 123, 90, 79 tubules for *Fbxo47-3FH* KI).

1006

1007 **Figure 3D** Testis sections (P18) were obtained from non-tagged control (3 animals) and  
1008 *Fbxo47-3FH* KI (3 animals). Number of seminiferous tubules that have HA+/*H1t+* cells was  
1009 counted per the seminiferous tubules that have *H1t+* spermatocyte cells (52, 36, 18 tubules for  
1010 non-tagged control; 15, 51, 36 tubules for *Fbxo47-3FH* KI).

1011

1012 **Figure 4C** Quantification of testes/body-weight ratio (mg/g) in *Fbxo47*<sup>+/-</sup> (8w; n=4) and  
1013 *Fbxo47* KO (8w; n=10) mice. n: the number of animals examined for each genotype. Bar graph  
1014 indicates mean with SD. Statistical significance was determined by t-test.

1015

1016 **Figure 4I** Cumulative number of pups born from *Fbxo47*<sup>+/-</sup> (n=4, all 6-week old at the start  
1017 point of mating) and *Fbxo47* KO (n=4, all 6-week old at the start point of mating) females was  
1018 counted for 18 weeks of breeding.

1019

1020 **Figure 5A** Quantification of the seminiferous tubules that have *H1t+*/*SYCP3+* cells per the  
1021 seminiferous tubules that have *SYCP3+* spermatocyte cells in *Fbxo47* heterozygous (p18: 62,  
1022 61, 29 tubules/animal were counted from n= 3 animals; 8w: 135, 143, 45 tubules/animal  
1023 were counted from n= 3 animals) and *Fbxo47* KO (p18: 105, 59, 141 tubules/animal were  
1024 counted from n= 3 animals; 8w: 36, 55, 63, 64, 88, 69, 108 tubules/animal were  
1025 counted from n= 7 animals) testes. n: the number of animals examined for each genotype. Bar  
1026 graph indicates mean with SD. Statistical significance was determined by unpaired t-test.  $p =$   
1027 0.0012 for *Fbxo47* heterozygous versus *Fbxo47* KO at P18.

1028

1029 **Figure 5C** Spermatocytes in the four developmental stages (leptotene, zygotene, pachytene, and  
1030 diplotene(-like)) per total cells in meiotic prophase were quantified in WT (n=727 from one  
1031 animal) and *Fbxo47* KO (n=659 from one animal) at P15, and in WT (n=561 from one animal)  
1032 and *Fbxo47* KO (n=516 from one animal) at P18.

1033

1034 **Figure 5F** Spermatocytes in the four developmental stages (leptotene or zygotene, pachytene,  
1035 and diplotene(-like)) per total cells in meiotic prophase were quantified in *Fbxo47*<sup>+/-</sup> (n=105  
1036 for OA -, 117 for OA+) and *Fbxo47* KO (n=140 for OA -, 117 for OA+).

1037

1038 **Figure 5G** Quantification of the seminiferous tubules that have TUNEL+ cells per total tubules  
1039 in *Fbxo47*<sup>+/-</sup> (8w: n=3) and *Fbxo47* KO (8w: n=3) testes. Bar graph indicates mean with SD.  
1040 Statistical significance was determined by t-test.

1041

1042 **Figure 6C** Numbers of RAD51 foci on *SYCP3* axes were counted in WT and *Fbxo47* KO.  
1043 Number of foci was indicated in the scatter plot with median. Statistical significance was  
1044 determined by Mann-Whitney U-test.

1045

1046 **Figure 6D** Numbers of MSH4 foci on SYCP3 axes were counted in WT and *Fbxo47* KO.  
1047 Number of foci was indicated in the scatter plot with median. Statistical significance was  
1048 determined by Mann-Whitney U-test.  
1049  
1050 **Figure 6E** Numbers of MLH1 foci on SYCP3 axes were counted in *Fbxo47*<sup>+/-</sup> pachyene  
1051 (n=15), or *Fbxo47* KO pachyene (n=13) and diplotene-like (n=13). Number of foci was  
1052 indicated in the scatter plot with median. Statistical significance was determined by  
1053 Mann-Whitney U-test.  
1054  
1055 **Figure S3D**  
1056 **Reference**  
  
1057 Antoine Baudrimont, Dimitra Paouneskou, Ariz Mohammad, Raffael  
  
1058 Lichtenberger, Joshua Blundon, Yumi Kim, Markus Hartl, Sebastian Falk, Tim  
  
1059 Schedl, and Jantsch, V. (2021). The CHK-2 antagonizing phosphatase PPM-1.D  
  
1060 regulates meiotic entry via catalytic and non-catalytic activities. bioRxiv.  
  
1061 [doi.org/10.1101/2021.08.02.453806](https://doi.org/10.1101/2021.08.02.453806).  
  
1062 Barbosa, P., Zhaunova, L., Debilio, S., Steccanella, V., Kelly, V., Ly, T., and  
  
1063 Ohkura, H. (2021). SCF-Fbxo42 promotes synaptonemal complex assembly by  
  
1064 downregulating PP2A-B56. *J Cell Biol* *220*. [10.1083/jcb.202009167](https://doi.org/10.1083/jcb.202009167).  
  
1065 Baudat, F., Imai, Y., and de Massy, B. (2013). Meiotic recombination in  
  
1066 mammals: localization and regulation. *Nat Rev Genet* *14*, 794-806.  
  
1067 [10.1038/nrg3573](https://doi.org/10.1038/nrg3573).

1068 Bisig, C.G., Guiraldelli, M.F., Kouznetsova, A., Scherthan, H., Hoog, C., Dawson,  
1069 D.S., and Pezza, R.J. (2012). Synaptonemal complex components persist at  
1070 centromeres and are required for homologous centromere pairing in mouse  
1071 spermatocytes. *PLoS Genet* *8*, e1002701. [10.1371/journal.pgen.1002701](https://doi.org/10.1371/journal.pgen.1002701).  
1072 Broering, T.J., Alavattam, K.G., Sadreyev, R.I., Ichijima, Y., Kato, Y., Hasegawa,  
1073 K., Camerini-Otero, R.D., Lee, J.T., Andreassen, P.R., and Namekawa, S.H.  
1074 (2014). BRCA1 establishes DNA damage signaling and pericentric  
1075 heterochromatin of the X chromosome in male meiosis. *J Cell Biol* *205*, 663-675.  
1076 [10.1083/jcb.201311050](https://doi.org/10.1083/jcb.201311050).  
1077 Cahoon, C.K., and Hawley, R.S. (2016). Regulating the construction and  
1078 demolition of the synaptonemal complex. *Nat Struct Mol Biol* *23*, 369-377.  
1079 [10.1038/nsmb.3208](https://doi.org/10.1038/nsmb.3208).  
1080 Cardozo, T., and Pagano, M. (2004). The SCF ubiquitin ligase: insights into a  
1081 molecular machine. *Nat Rev Mol Cell Biol* *5*, 739-751. [10.1038/nrm1471](https://doi.org/10.1038/nrm1471).  
1082 Chen, Y., Zheng, Y., Gao, Y., Lin, Z., Yang, S., Wang, T., Wang, Q., Xie, N., Hua,  
1083 R., Liu, M., et al. (2018). Single-cell RNA-seq uncovers dynamic processes and

- 1084 critical regulators in mouse spermatogenesis. *Cell Res* *28*, 879-896.
- 1085 10.1038/s41422-018-0074-y.
- 1086 Cloud, V., Chan, Y.L., Grubb, J., Budke, B., and Bishop, D.K. (2012). Rad51 is  
1087 an accessory factor for Dmc1-mediated joint molecule formation during meiosis.  
1088 *Science* *337*, 1222-1225. 10.1126/science.1219379.
- 1089 Cobb, J., Cargile, B., and Handel, M.A. (1999). Acquisition of competence to  
1090 condense metaphase I chromosomes during spermatogenesis. *Dev Biol* *205*,  
1091 49-64. 10.1006/dbio.1998.9101.
- 1092 Daniel, K., Lange, J., Hached, K., Fu, J., Anastassiadis, K., Roig, I., Cooke, H.J.,  
1093 Stewart, A.F., Wassmann, K., Jasin, M., et al. (2011). Meiotic homologue  
1094 alignment and its quality surveillance are controlled by mouse HORMAD1. *Nat*  
1095 *Cell Biol* *13*, 599-610. 10.1038/ncb2213.
- 1096 Deshaies, R.J. (1999). SCF and Cullin/Ring H2-based ubiquitin ligases. *Annu*  
1097 *Rev Cell Dev Biol* *15*, 435-467. 10.1146/annurev.cellbio.15.1.435.

- 1098 Drabent, B., Bode, C., Bramlage, B., and Doenecke, D. (1996). Expression of  
1099 the mouse testicular histone gene H1t during spermatogenesis. *Histochem Cell*  
1100 *Biol* *106*, 247-251. [10.1007/BF02484408](https://doi.org/10.1007/BF02484408).
- 1101 Guan, Y., Leu, N.A., Ma, J., Chmatal, L., Ruthel, G., Bloom, J.C., Lampson, M.A.,  
1102 Schimenti, J.C., Luo, M., and Wang, P.J. (2020). SKP1 drives the prophase I to  
1103 metaphase I transition during male meiosis. *Sci Adv* *6*, eaaz2129.  
1104 [10.1126/sciadv.aaz2129](https://doi.org/10.1126/sciadv.aaz2129).
- 1105 He, Y., Wang, C., Higgins, J.D., Yu, J., Zong, J., Lu, P., Zhang, D., and Liang, W.  
1106 (2016). MEIOTIC F-BOX Is Essential for Male Meiotic DNA Double-Strand Break  
1107 Repair in Rice. *Plant Cell* *28*, 1879-1893. [10.1105/tpc.16.00108](https://doi.org/10.1105/tpc.16.00108).
- 1108 Hermann, B.P., Cheng, K., Singh, A., Roa-De La Cruz, L., Mutoji, K.N., Chen,  
1109 I.C., Gildersleeve, H., Lehle, J.D., Mayo, M., Westernstroer, B., et al. (2018). The  
1110 Mammalian Spermatogenesis Single-Cell Transcriptome, from Spermatogonial  
1111 Stem Cells to Spermatids. *Cell Rep* *25*, 1650-1667 e1658.  
1112 [10.1016/j.celrep.2018.10.026](https://doi.org/10.1016/j.celrep.2018.10.026).

- 1113 Horisawa-Takada, Y., Kodera, C., Takemoto, K., Sakashita, A., Horisawa, K.,
- 1114 Maeda, R., Shimada, R., Usuki, S., Fujimura, S., Tani, N., et al. (2021).
- 1115 Meiosis-specific ZFP541 repressor complex promotes developmental
- 1116 progression of meiotic prophase towards completion during mouse
- 1117 spermatogenesis. *Nature Communications* *12*, 3184.
- 1118 [10.1038/s41467-021-23378-4](https://doi.org/10.1038/s41467-021-23378-4).
- 1119 Hua, R., Wei, H., Liu, C., Zhang, Y., Liu, S., Guo, Y., Cui, Y., Zhang, X., Guo, X.,
- 1120 Li, W., and Liu, M. (2019). FBXO47 regulates telomere-inner nuclear envelope
- 1121 integration by stabilizing TRF2 during meiosis. *Nucleic Acids Res* *47*,
- 1122 11755-11770. [10.1093/nar/gkz992](https://doi.org/10.1093/nar/gkz992).
- 1123 Ishiguro, K., Kim, J., Fujiyama-Nakamura, S., Kato, S., and Watanabe, Y. (2011).
- 1124 A new meiosis-specific cohesin complex implicated in the cohesin code for
- 1125 homologous pairing. *EMBO Rep* *12*, 267-275. [10.1038/embor.2011.2](https://doi.org/10.1038/embor.2011.2).
- 1126 Ishiguro, K., Kim, J., Shibuya, H., Hernandez-Hernandez, A., Suzuki, A.,
- 1127 Fukagawa, T., Shioi, G., Kiyonari, H., Li, X.C., Schimenti, J., et al. (2014).

- 1128 Meiosis-specific cohesin mediates homolog recognition in mouse spermatocytes.
- 1129 *Genes Dev* *28*, 594-607. 10.1101/gad.237313.113.
- 1130 Ishiguro, K.I., Matsuura, K., Tani, N., Takeda, N., Usuki, S., Yamane, M.,
- 1131 Sugimoto, M., Fujimura, S., Hosokawa, M., Chuma, S., et al. (2020). MEIOSIN
- 1132 Directs the Switch from Mitosis to Meiosis in Mammalian Germ Cells. *Dev Cell*
- 1133 *52*, 429-445 e410. 10.1016/j.devcel.2020.01.010.
- 1134 Jantsch, V., Tang, L., Pasierbek, P., Penkner, A., Nayak, S., Baudrimont, A.,
- 1135 Schedl, T., Gartner, A., and Loidl, J. (2007). *Caenorhabditis elegans* prom-1 is
- 1136 required for meiotic prophase progression and homologous chromosome pairing.
- 1137 *Mol Biol Cell* *18*, 4911-4920. 10.1091/mbc.e07-03-0243.
- 1138 Jin, J., Cardozo, T., Lovering, R.C., Elledge, S.J., Pagano, M., and Harper, J.W.
- 1139 (2004). Systematic analysis and nomenclature of mammalian F-box proteins.
- 1140 *Genes Dev* *18*, 2573-2580. 10.1101/gad.1255304.
- 1141 Jordan, P.W., Karppinen, J., and Handel, M.A. (2012). Polo-like kinase is
- 1142 required for synaptonemal complex disassembly and phosphorylation in mouse
- 1143 spermatocytes. *J Cell Sci* *125*, 5061-5072. 10.1242/jcs.105015.



- 1144 Keeney, S., Lange, J., and Mohibullah, N. (2014). Self-organization of meiotic  
1145 recombination initiation: general principles and molecular pathways. *Annu Rev*  
1146 *Genet* *48*, 187-214. [10.1146/annurev-genet-120213-092304](https://doi.org/10.1146/annurev-genet-120213-092304).
- 1147 Kikuchi, M., Nishimura, T., Ishishita, S., Matsuda, Y., and Tanaka, M. (2020).  
1148 *foxl3*, a sexual switch in germ cells, initiates two independent molecular  
1149 pathways for commitment to oogenesis in medaka. *Proc Natl Acad Sci U S A*  
1150 *117*, 12174-12181. [10.1073/pnas.1918556117](https://doi.org/10.1073/pnas.1918556117).
- 1151 Kipreos, E.T., and Pagano, M. (2000). The F-box protein family. *Genome Biol* *1*,  
1152 *REVIEWS3002*. [10.1186/gb-2000-1-5-reviews3002](https://doi.org/10.1186/gb-2000-1-5-reviews3002).
- 1153 Kojima, M.L., de Rooij, D.G., and Page, D.C. (2019). Amplification of a broad  
1154 transcriptional program by a common factor triggers the meiotic cell cycle in  
1155 mice. *Elife* *8*. [10.7554/eLife.43738](https://doi.org/10.7554/eLife.43738).
- 1156 Mahadevaiah, S.K., Turner, J.M., Baudat, F., Rogakou, E.P., de Boer, P.,  
1157 Blanco-Rodriguez, J., Jasin, M., Keeney, S., Bonner, W.M., and Burgoyne, P.S.  
1158 (2001). Recombinational DNA double-strand breaks in mice precede synapsis.  
1159 *Nat Genet* *27*, 271-276. [10.1038/85830](https://doi.org/10.1038/85830).

- 1160 Mohammad, A., Vanden Broek, K., Wang, C., Daryabeigi, A., Jantsch, V.,  
1161 Hansen, D., and Schedl, T. (2018). Initiation of Meiotic Development Is  
1162 Controlled by Three Post-transcriptional Pathways in *Caenorhabditis elegans*.  
1163 *Genetics* *209*, 1197-1224. 10.1534/genetics.118.300985.
- 1164 Parra, M.T., Gomez, R., Viera, A., Llano, E., Pendas, A.M., Rufas, J.S., and Suja,  
1165 J.A. (2009). Sequential assembly of centromeric proteins in male mouse meiosis.  
1166 *PLoS Genet* *5*, e1000417. 10.1371/journal.pgen.1000417.
- 1167 Parra, M.T., Viera, A., Gomez, R., Page, J., Carmena, M., Earnshaw, W.C.,  
1168 Rufas, J.S., and Suja, J.A. (2003). Dynamic relocalization of the chromosomal  
1169 passenger complex proteins inner centromere protein (INCENP) and aurora-B  
1170 kinase during male mouse meiosis. *J Cell Sci* *116*, 961-974. 10.1242/jcs.00330.
- 1171 Peters, A.H., Plug, A.W., van Vugt, M.J., and de Boer, P. (1997). A drying-down  
1172 technique for the spreading of mammalian meiocytes from the male and female  
1173 germline. *Chromosome Res* *5*, 66-68.
- 1174 Qiao, H., Chen, J.K., Reynolds, A., Hoog, C., Paddy, M., and Hunter, N. (2012).  
1175 Interplay between synaptonemal complex, homologous recombination, and

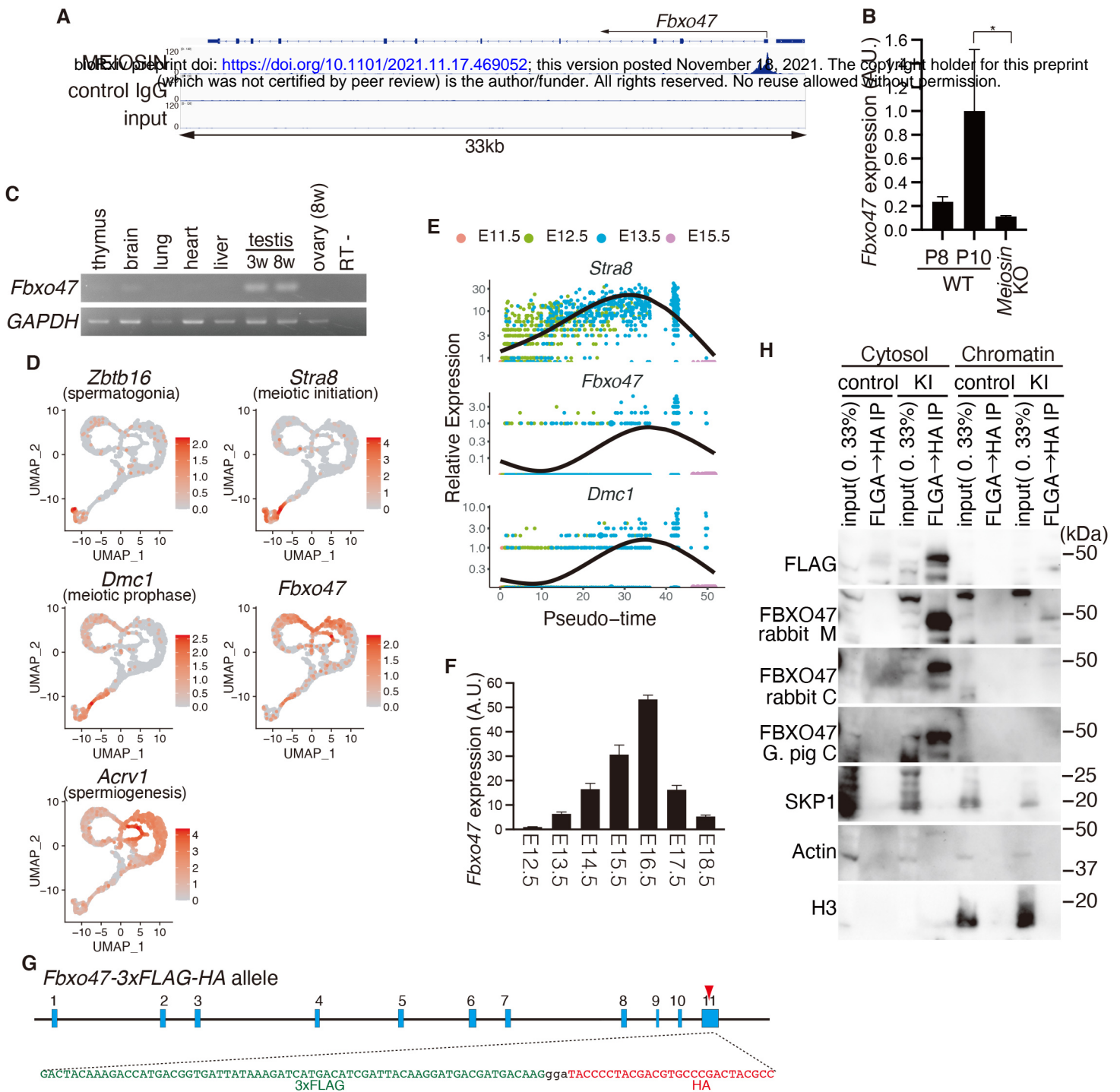
- 1176 centromeres during mammalian meiosis. *PLoS Genet* *8*, e1002790.
- 1177 [10.1371/journal.pgen.1002790](https://doi.org/10.1371/journal.pgen.1002790).
- 1178 Qiu, X., Hill, A., Packer, J., Lin, D., Ma, Y.A., and Trapnell, C. (2017). Single-cell  
1179 mRNA quantification and differential analysis with Census. *Nat Methods* *14*,  
1180 309-315. [10.1038/nmeth.4150](https://doi.org/10.1038/nmeth.4150).
- 1181 Reitsma, J.M., Liu, X., Reichermeier, K.M., Moradian, A., Sweredoski, M.J.,  
1182 Hess, S., and Deshaies, R.J. (2017). Composition and Regulation of the Cellular  
1183 Repertoire of SCF Ubiquitin Ligases. *Cell* *171*, 1326-1339 e1314.  
1184 [10.1016/j.cell.2017.10.016](https://doi.org/10.1016/j.cell.2017.10.016).
- 1185 Royo, H., Prosser, H., Ruzankina, Y., Mahadevaiah, S.K., Cloutier, J.M.,  
1186 Baumann, M., Fukuda, T., Hoog, C., Toth, A., de Rooij, D.G., et al. (2013). ATR  
1187 acts stage specifically to regulate multiple aspects of mammalian meiotic  
1188 silencing. *Genes Dev* *27*, 1484-1494. [10.1101/gad.219477.113](https://doi.org/10.1101/gad.219477.113).
- 1189 Scully, R., Chen, J., Plug, A., Xiao, Y., Weaver, D., Feunteun, J., Ashley, T., and  
1190 Livingston, D.M. (1997). Association of BRCA1 with Rad51 in mitotic and meiotic  
1191 cells. *Cell* *88*, 265-275. [10.1016/s0092-8674\(00\)81847-4](https://doi.org/10.1016/s0092-8674(00)81847-4).

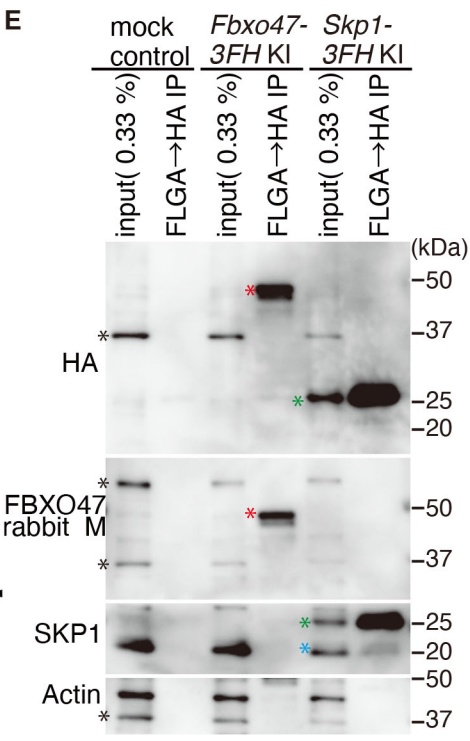
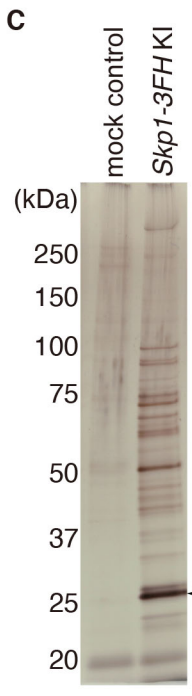
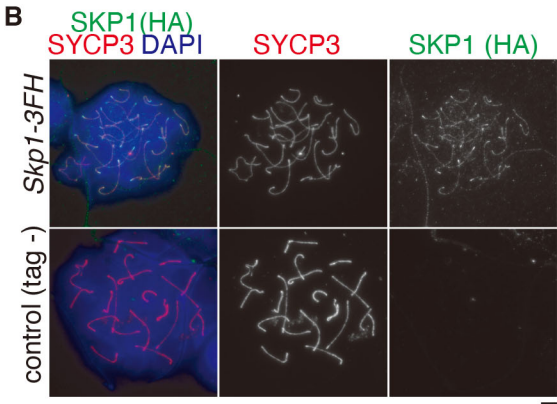
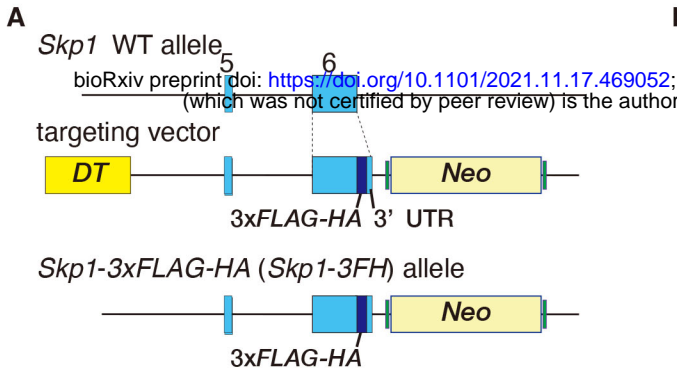
- 1192 Shibuya, H., Ishiguro, K., and Watanabe, Y. (2014). The TRF1-binding protein  
1193 TERB1 promotes chromosome movement and telomere rigidity in meiosis. *Nat*  
1194 *Cell Biol* *16*, 145-156. 10.1038/ncb2896.
- 1195 Shimada, R., Koike, H., Hirano, T., Kato, Y., and Saga, Y. (2021). NANOS2  
1196 suppresses the cell cycle by repressing mTORC1 activators in embryonic male  
1197 germ cells. *iScience* *24*, 102890. 10.1016/j.isci.2021.102890.
- 1198 Shin, Y.H., Choi, Y., Erdin, S.U., Yatsenko, S.A., Kloc, M., Yang, F., Wang, P.J.,  
1199 Meistrich, M.L., and Rajkovic, A. (2010). Hormad1 mutation disrupts  
1200 synaptonemal complex formation, recombination, and chromosome segregation  
1201 in mammalian meiosis. *PLoS Genet* *6*, e1001190.  
1202 10.1371/journal.pgen.1001190.
- 1203 Shinohara, A., and Shinohara, M. (2004). Roles of RecA homologues Rad51  
1204 and Dmc1 during meiotic recombination. *Cytogenet Genome Res* *107*, 201-207.  
1205 10.1159/000080598.
- 1206 Stuart, T., Butler, A., Hoffman, P., Hafemeister, C., Papalexi, E., Mauck, W.M.,  
1207 3rd, Hao, Y., Stoeckius, M., Smibert, P., and Satija, R. (2019). Comprehensive

- 1208 Integration of Single-Cell Data. *Cell* *177*, 1888-1902 e1821.
- 1209 [10.1016/j.cell.2019.05.031](https://doi.org/10.1016/j.cell.2019.05.031).
- 1210 Takemoto, K., Tani, N., Takada-Horisawa, Y., Fujimura, S., Tanno, N., Yamane,  
1211 M., Okamura, K., Sugimoto, M., Araki, K., and Ishiguro, K.-i. (2020).
- 1212 Meiosis-Specific C19orf57/4930432K21Rik/BRME1 Modulates Localization of  
1213 RAD51 and DMC1 to DSBs in Mouse Meiotic Recombination. *Cell Reports* *31*,  
1214 107686. <https://doi.org/10.1016/j.celrep.2020.107686>.
- 1215 Turner, J.M., Aprelikova, O., Xu, X., Wang, R., Kim, S., Chandramouli, G.V.,  
1216 Barrett, J.C., Burgoyne, P.S., and Deng, C.X. (2004). BRCA1, histone H2AX  
1217 phosphorylation, and male meiotic sex chromosome inactivation. *Curr Biol* *14*,  
1218 2135-2142. [10.1016/j.cub.2004.11.032](https://doi.org/10.1016/j.cub.2004.11.032).
- 1219 Wiltshire, T., Park, C., Caldwell, K.A., and Handel, M.A. (1995). Induced  
1220 premature G2/M-phase transition in pachytene spermatocytes includes events  
1221 unique to meiosis. *Dev Biol* *169*, 557-567. [10.1006/dbio.1995.1169](https://doi.org/10.1006/dbio.1995.1169).
- 1222 Wojtasz, L., Daniel, K., Roig, I., Bolcun-Filas, E., Xu, H., Boonsanay, V.,  
1223 Eckmann, C.R., Cooke, H.J., Jasin, M., Keeney, S., et al. (2009). Mouse

- 1224   HORMAD1 and HORMAD2, two conserved meiotic chromosomal proteins, are
- 1225   depleted from synapsed chromosome axes with the help of TRIP13
- 1226   AAA-ATPase. *PLoS Genet* *5*, e1000702. [10.1371/journal.pgen.1000702](https://doi.org/10.1371/journal.pgen.1000702).
- 1227   Zhang, F., Tang, D., Shen, Y., Xue, Z., Shi, W., Ren, L., Du, G., Li, Y., and
- 1228   Cheng, Z. (2017). The F-Box Protein ZYGO1 Mediates Bouquet Formation to
- 1229   Promote Homologous Pairing, Synapsis, and Recombination in Rice Meiosis.
- 1230   *Plant Cell* *29*, 2597-2609. [10.1105/tpc.17.00287](https://doi.org/10.1105/tpc.17.00287).
- 1231   Zhu, Z., Bani Ismail, M., Shinohara, M., and Shinohara, A. (2021). SCF(Cdc4)
- 1232   ubiquitin ligase regulates synaptonemal complex formation during meiosis. *Life*
- 1233   *Sci Alliance* *4*. [10.26508/lsa.202000933](https://doi.org/10.26508/lsa.202000933).
- 1234   Zickler, D., and Kleckner, N. (2015). Recombination, Pairing, and Synapsis of
- 1235   Homologs during Meiosis. *Cold Spring Harb Perspect Biol* *7*.
- 1236   [10.1101/cshperspect.a016626](https://doi.org/10.1101/cshperspect.a016626).
- 1237

Figure 1

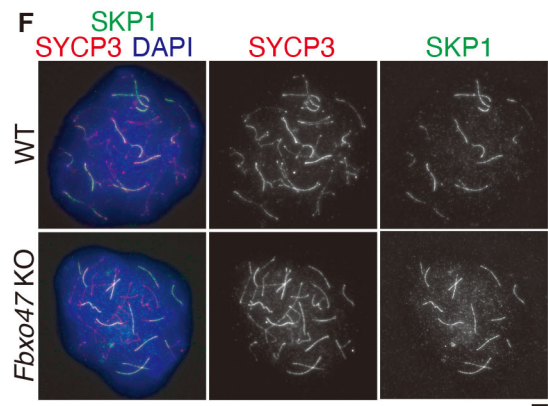




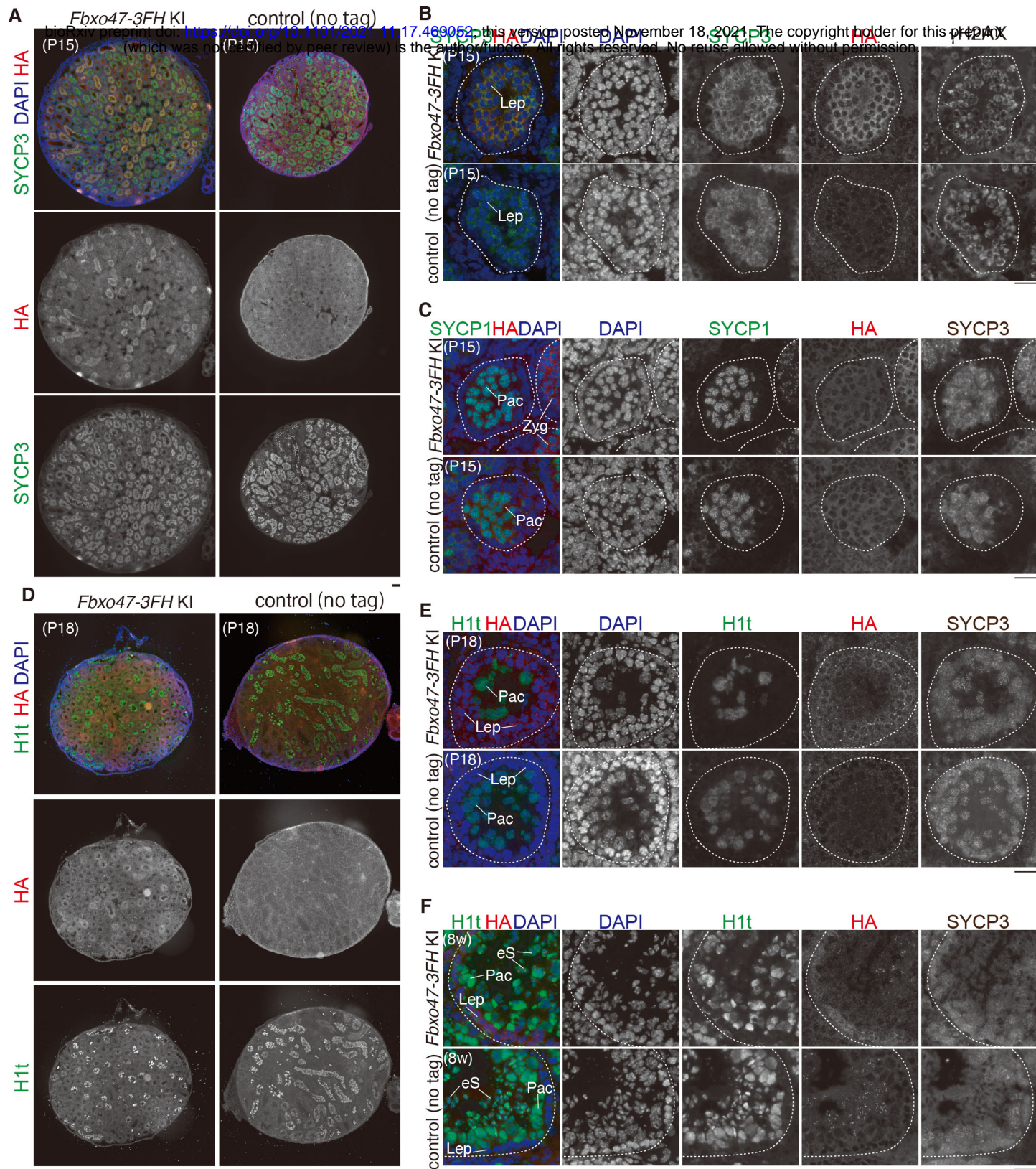
**D**

this version posted November 18, 2021. The copyright holder for this preprint (which was not certified by peer review) is the author/funder. All rights reserved. No reuse allowed without permission.

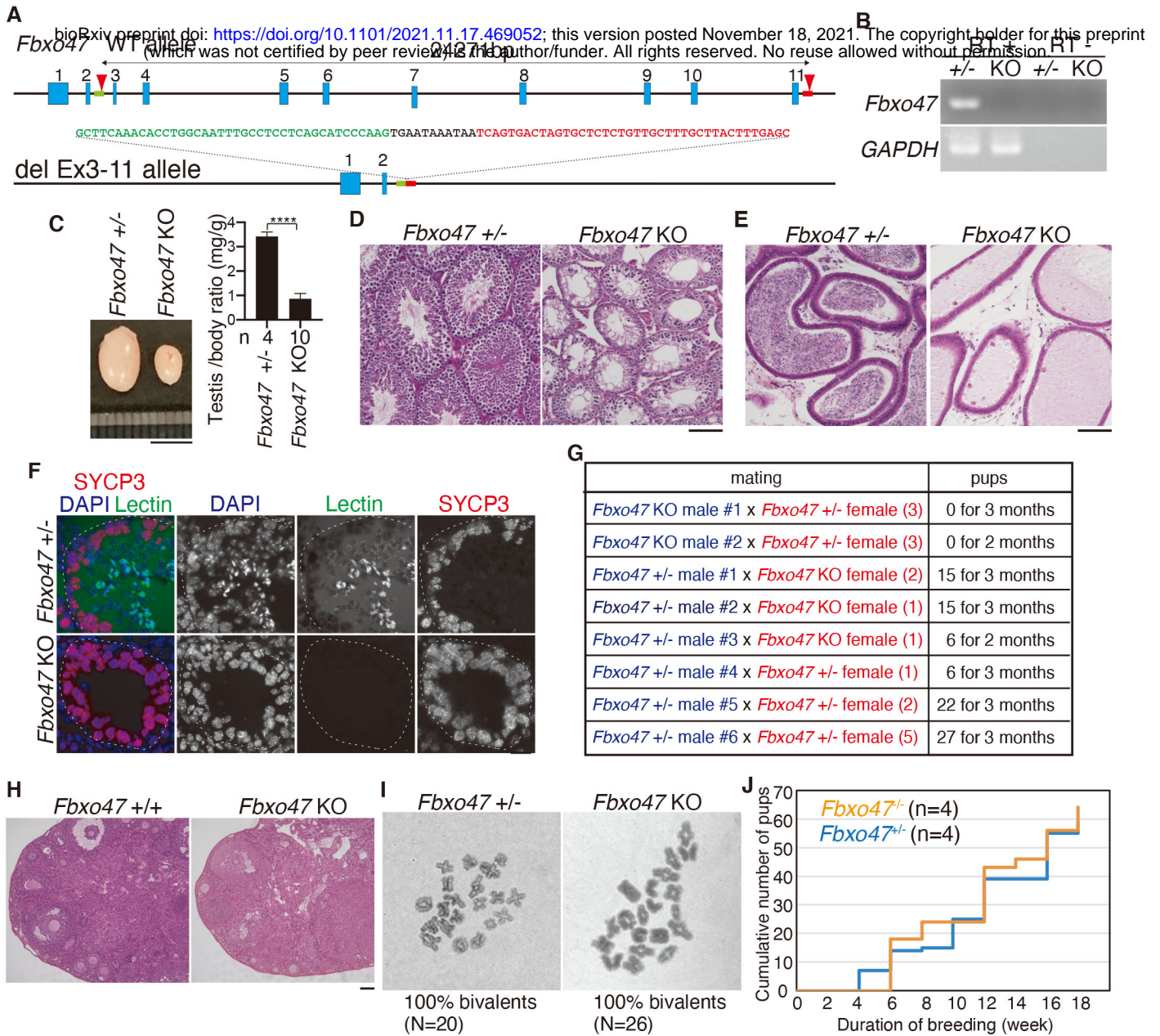
Accession	Protein	Score	PSMs
Q9WFX6	Cullin-1 [CUL1]	776	5016.17
Q9DC63	F-box only protein 3 [FBX3]	480	2411.23
F8VPX2	F-box and WD-40 domain protein 9 [FBXW9]	458	2036.05
Q5SUR3	S-phase kinase-associated protein 1 [SKP1a]	163	1800.62
F8VQK6	F-box and leucine-rich repeat protein 18 [FBXL18]	707	1717.66
Q6PB97	F-box/LRR-repeat protein 19 [FXL19]	674	1675.94
Q9QXW2	F-box/WD repeat-containing protein 5 [FBXW5]	573	1529.59
Q5SR7	F-box/WD repeat-containing protein 11 [FBW1B]	542	1207.27
Q3ULA2	F-box/WD repeat-containing protein 1A [FBW1A]	605	1030.81
Q79JE5	F-box only protein 22 [FBX22]	402	856.45
Q8BK06	F-box only protein 9 [FBX9]	437	836.21
Q60584	F-box/WD repeat-containing protein 2 [FBXW2]	422	720.79
Q3TNG8	F-box only protein 42 [FBX42]	705	638.83
Q3U7U3	F-box only protein 7 [FBX7]	523	594.01
Q8BIA4	F-box/WD repeat-containing protein 8 [FBXW8]	598	588.11
Q7TQF2	F-box only protein 10 [FBX10]	950	581.03
F6YRW4	F-box and leucine-rich repeat protein 11 [KDM2A/FBXL11]	1161	537.74
Q91W61	F-box/LRR-repeat protein 15 [FXL15]	300	457.56
Q9CQ24	F-box only protein 36 [FBX36]	188	444.49
Q8BJL1	F-box only protein 30 [FBX30]	746	436.85
Q9QZNI	F-box/LRR-repeat protein 17 [FXL17]	701	336.99
Q8CHQ0	F-box only protein 4 [FBX4]	385	285.02
D3YVU7	Lysine-specific demethylase 2B [KDM2B/FBXL10]	1254	274.35
Q7TPD1	F-box only protein 11 [FBX11]	930	220.42
Q80UW2	F-box only protein 2 [FBX2]	297	193.40
Q8CFE8	F-box and WD-40 domain protein 17 [FBXW17]	466	191.40
Q9CZV8	F-box/LRR-repeat protein 20 [FXL20]	436	165.19
Q8CIG9	F-box/LRR-repeat protein 8 [FBXL8]	374	157.74
A0A494BAM1	F-box only protein 15 [FBX15]	512	151.61
D3YUA8	F-box/WD repeat-containing protein 7 [FBXW7]	589	151.28
Q9EPX5	F-box/LRR-repeat protein 12 [FXL12]	326	150.50
Q8BH70	F-box/LRR-repeat protein 4 [FBXL4]	621	144.94
Q8C7B6	F-box and leucine-rich repeat protein 22 [FXL22]	236	144.84
Q8BG80	F-box only protein 46 [FBX46]	603	133.83
Q8BI64	F-box only protein 28 [FBX28]	368	124.56
Q8BMI0	F-box only protein 38 [FBX38]	1194	118.51
Q569Z9	S-phase kinase-associated protein 2 [SKP2/FBL1]	424	112.11
Q9D2Y6	F-box only protein 25 [FBX25]	357	110.36
Q3TJJ7	F-box/LRR-repeat protein 3 [FBXL3]	428	98.29
Q8BID8	F-box/LRR-repeat protein 14 [FXL14]	400	83.87
A9C491	Cullin-7 [CUL7]	1689	82.37
Q3V1V2	F-box only protein 33 [FBX33]	296	66.44
Q3TQF0	F-box only protein 31 [FBX31]	507	58.48
B2RPY3	F-box/LRR-repeat protein 16 [FXL16]	479	55.21
P51944	Cyclin-F [CCNF/FBXO1]	777	51.20
A0A2R8W6G1	E3 ubiquitin-protein ligase RBX1 [RBX1]	59	23.63

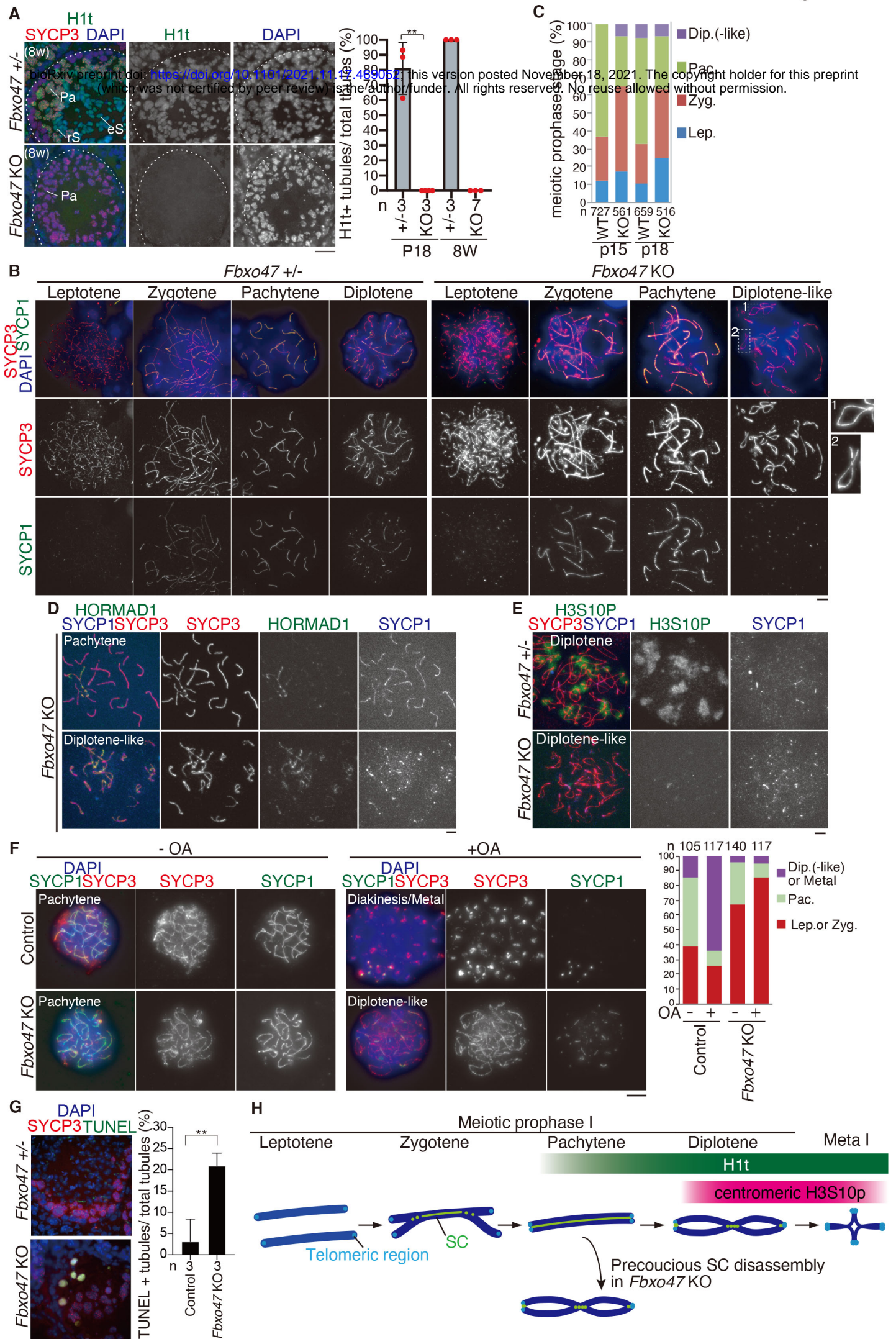


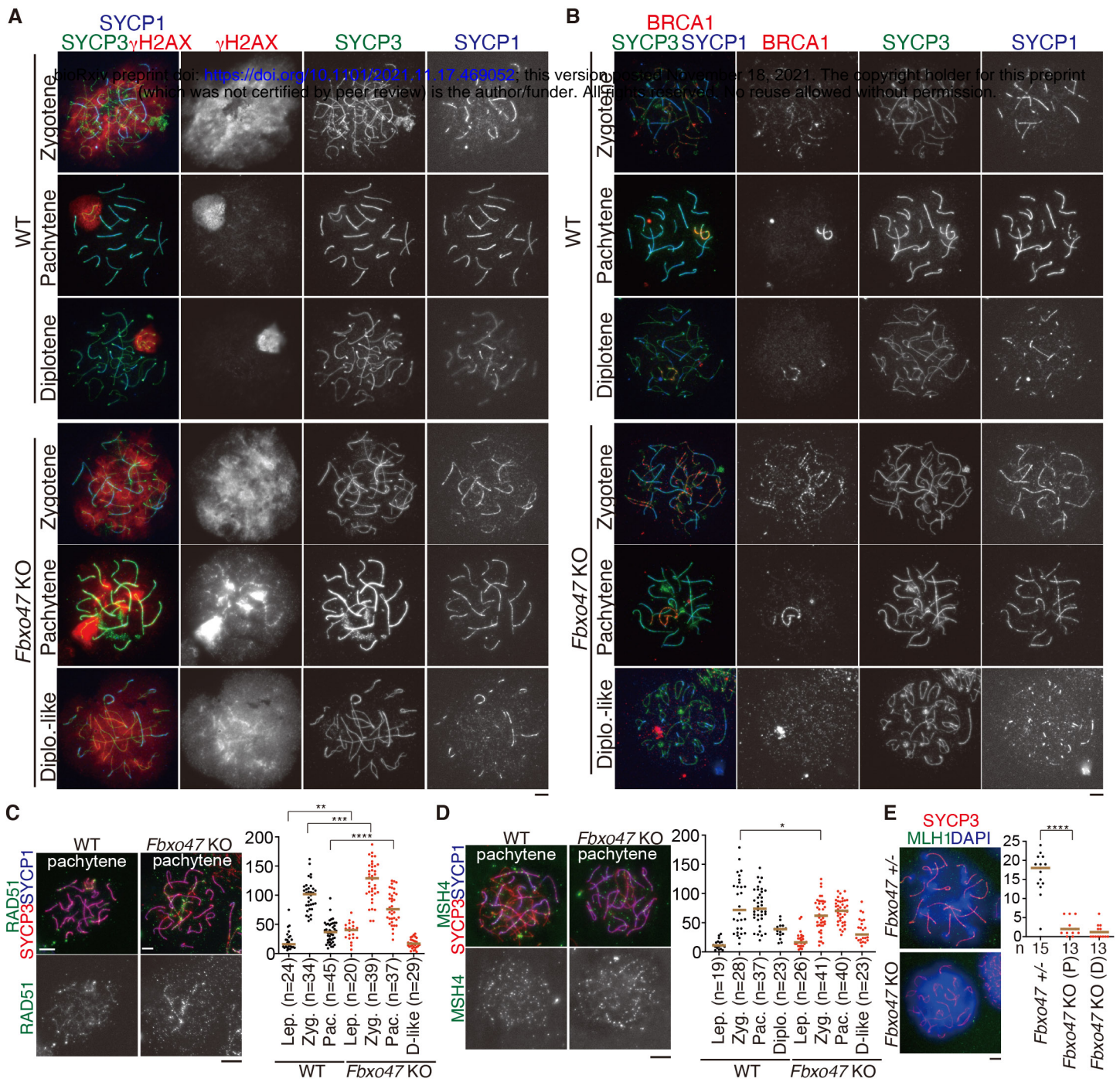




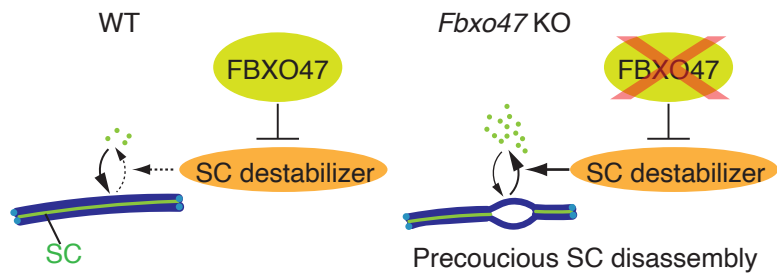
bioRxiv preprint doi: <https://doi.org/10.1101/2021.11.17.469053>; this version posted November 18, 2021. The copyright holder for this preprint (which was not certified by peer review) is the author/funder. All rights reserved. No reuse allowed without permission.



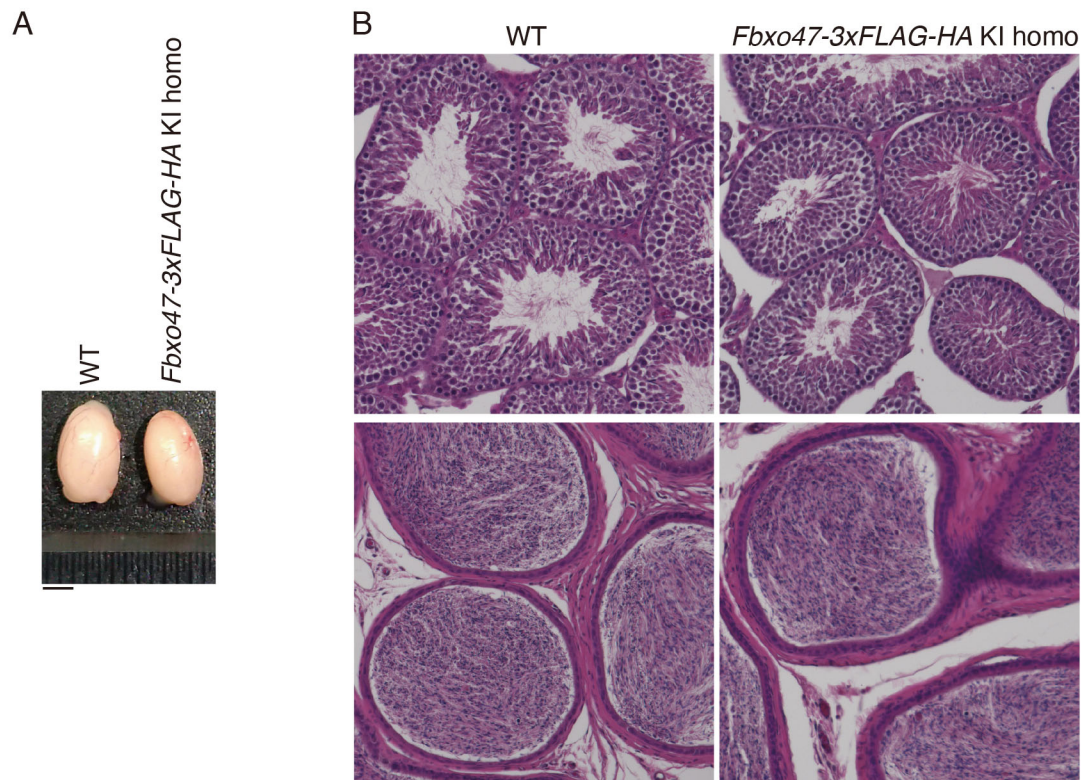




bioRxiv preprint doi: <https://doi.org/10.1101/2021.11.17.469052>; this version posted November 18, 2021. The copyright holder for this preprint (which was not certified by peer review) is the author/funder. All rights reserved. No reuse allowed without permission.



bioRxiv preprint doi: <https://doi.org/10.1101/2021.11.17.469052>; this version posted November 18, 2021. The copyright holder for this preprint (which was not certified by peer review) is the author/funder. All rights reserved. No reuse allowed without permission.



**Supplementary Figure 1. Generation of *Fbxo47-3xFLAG-HA* knock-in mice (related to Figure 1)**

**(A)** Testes from WT (no-tagged) and the *Fbxo47-3xFLAG-HA* KI homozygous mice (8-weeks old). Scale bar: 5 mm.

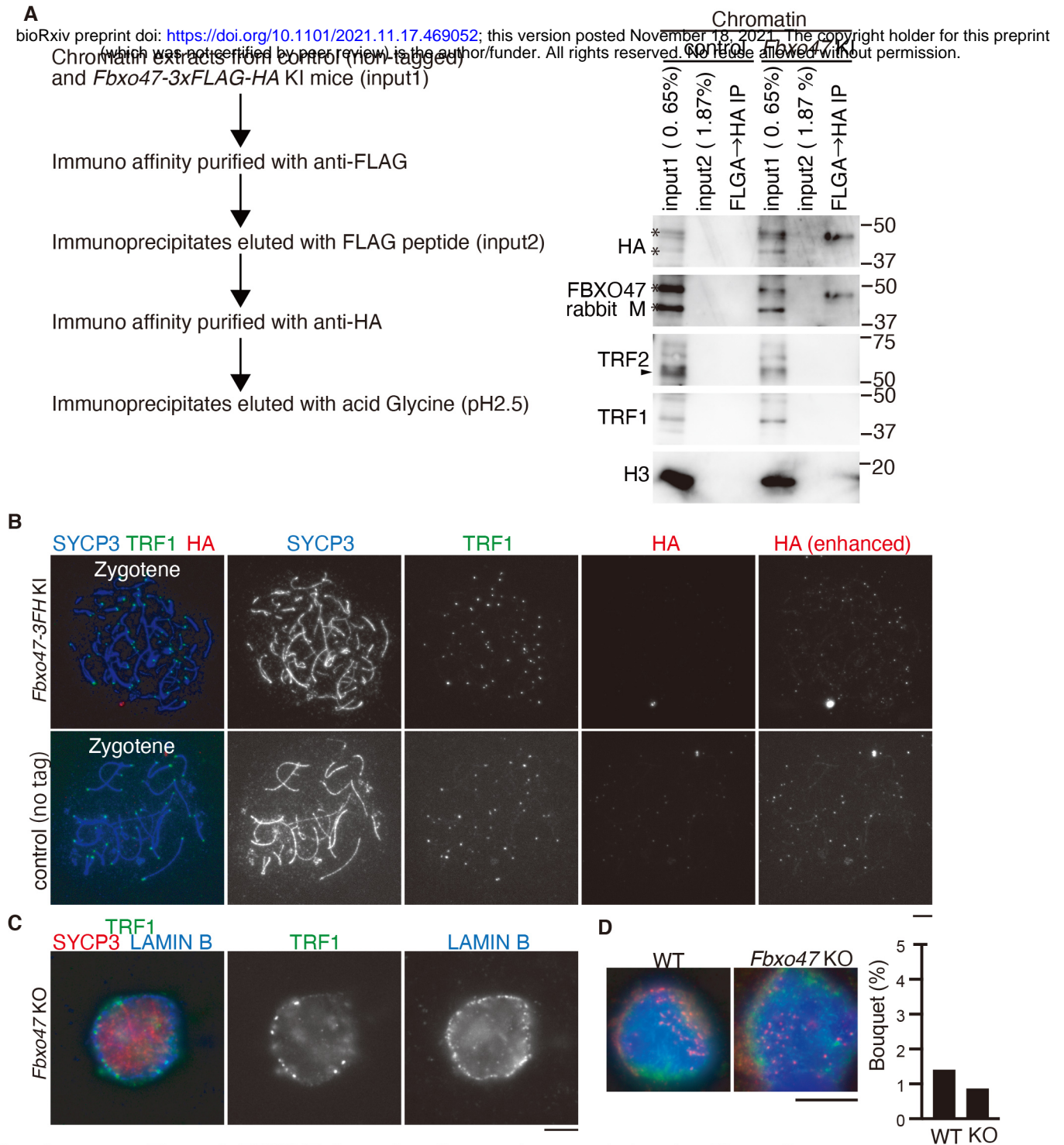
**(B)** Hematoxylin and eosin staining of the testes (upper) and epididymis (lower) sections from WT (non-tagged control) and the *Fbxo47-3xFLAG-HA* KI homozygous testes (8-weeks old). Scale bar: 100  $\mu$ m.

Note that The FBOX47-3xFLAG-HA fusion protein was physiologically functional considering the normal fertility shown in homozygous male and female mice with the KI allele.

Accession	Description	FBXO47-3xFLAG-HA IP from cytosol	
		Score	PSMs
P16546	<b>Spectrin alpha chain (Sptan1)</b>	700.00	34
A2A6H3	<b>F-box only protein 47 (Fbxo47)</b>	396.96	17
Q3UDF8	<b>eukaryotic translation initiation factor 2, subunit 3, structural gene X-linked (Eif2s3x)</b>	139.60	5
Q61749	<b>Translation initiation factor eIF-2B subunit delta (Eif2b4)</b>	112.64	6
Q8VDD5	<b>Myosin-9 (Myh9)</b>	100.59	7
Q8BP92	<b>Reticulocalbin-2 (Rcn2)</b>	94.35	4
A0AUM9	<b>Eif2b3 protein (Eif2b3)</b>	82.91	5
Q3TQP7	<b>acetyl-Coenzyme A acetyltransferase 1 (Acat1)</b>	76.43	3
P43275	<b>Histone H1.1 (Hist1h1a)</b>	71.91	3
Q6ZPE2	<b>Myotubularin-related protein 5 (Sbf1)</b>	66.18	3
Q99L45	<b>Eukaryotic translation initiation factor 2 subunit 2 (Eif2s2)</b>	60.83	3
Q9CSU2	<b>26S proteasome regulatory subunit RPN11 (Psm14)</b>	57.53	3
Q922W7	<b>2900073G15Rik protein (Myl12a)</b>	55.52	2
D6RFB8	<b>DNA polymerase (Pold1)</b>	54.02	4
Q91XU3	<b>Phosphatidylinositol 5-phosphate 4-kinase type-2 gamma (Pip4k2c)</b>	49.04	2
Q99LD9	<b>DnaJ homolog subfamily A member 1 (Dnaja1)</b>	48.43	3
Q7M754	<b>Try10-like trypsinogen (Gm5409)</b>	45.86	6
P63037	<b>DnaJ homolog subfamily A member 1 (Dnaja1)</b>	45.20	3
Q63ZW9	<b>Copa protein (Copa)</b>	43.81	3
Q80VC9	<b>Calmodulin-regulated spectrin-associated protein 3 (Camsap3)</b>	40.34	2
Q8BJY1	<b>26S proteasome non-ATPase regulatory subunit 5 (Psm5)</b>	33.62	2
B2RXC6	<b>DNA-directed RNA polymerase subunit (Polr3a)</b>	31.02	3
Q68FL6	<b>Methionine--tRNA ligase, cytoplasmic (Mars)</b>	29.26	2
Q3U1G4	<b>Sec3-PIP2_bind domain-containing protein (Exoc1)</b>	28.42	2
Q925I1	<b>ATPase family AAA domain-containing protein 3 (Atad3)</b>	23.98	2
A0A3B2WBH9	<b>Tight junction protein ZO-2 (Tjp2)</b>	21.72	2
F6ZQQ3	<b>26S proteasome non-ATPase regulatory subunit 13 (Psm13)</b>	21.36	2

**Supplementary Figure 2. MS analyses of FBXO47 interacting factors in testis extracts (related to Figure 1)**

The immunoprecipitates (IP) from the cytosolic fraction of the testis extracts were subjected to liquid chromatography tandem-mass spectrometry (LC-MS/MS) analyses. The proteins identified by the LC-MS/MS analysis of FBXO47-IP are presented after excluding the proteins detected in the control IgG-IP. The proteins with more than 1 different peptide hits are listed with UniProt accession number, the number of peptide hits and Mascot scores.



### Supplementary Figure 3. FBXO47 do not localize to telomeres (related to Figure 1)

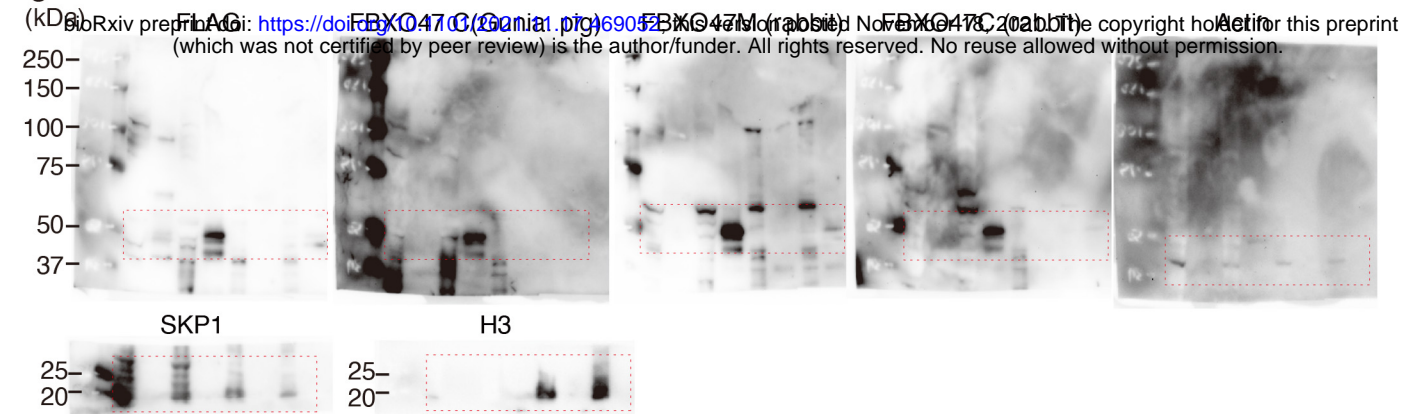
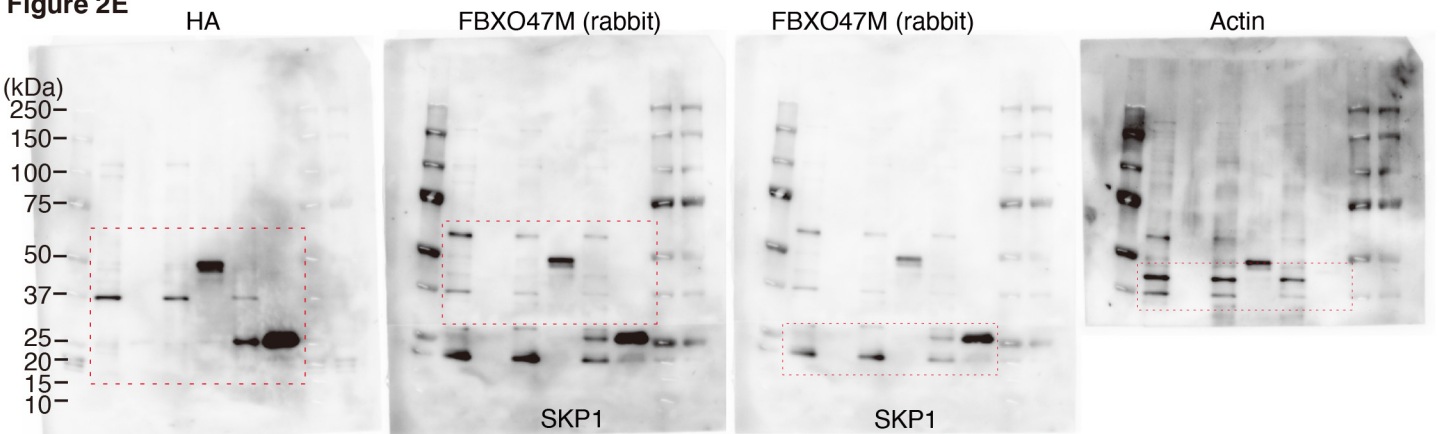
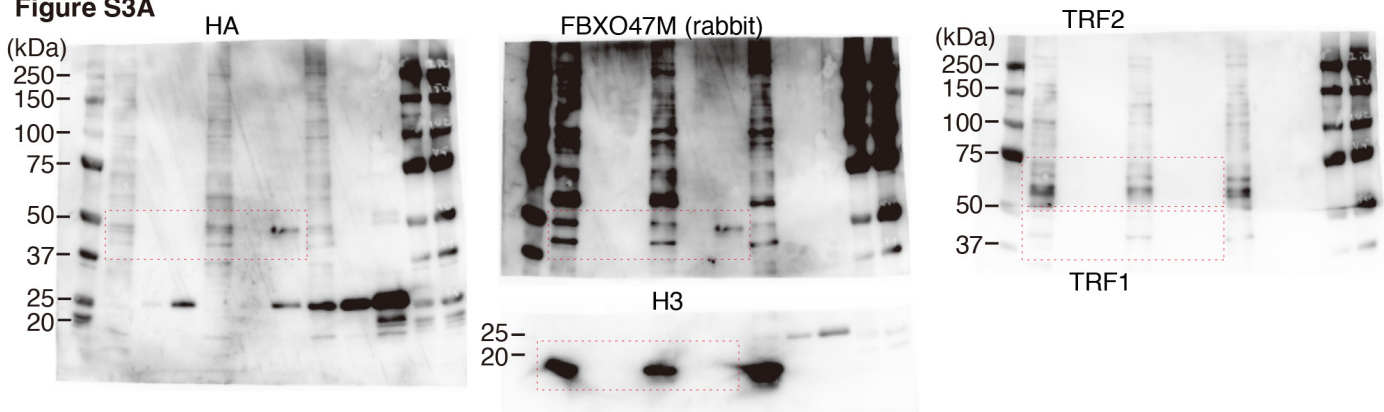
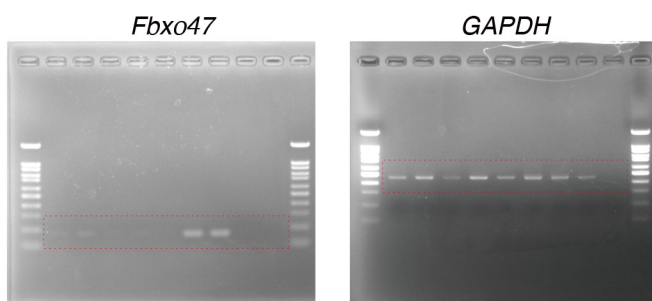
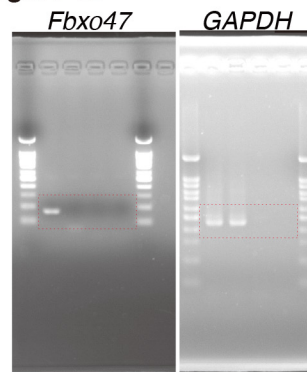
(A) Western blot showed immunoprecipitates from chromatin extracts of WT (non-tagged control) and *Fbxo47-3FH* KI mouse testes (from 139 and 148 animals at P14-19, respectively) after tandem affinity purifications using anti-FLAG and anti-HA antibodies. The same membrane was sequentially reblotted with different antibodies as indicated. \*: non-specific band. Arrowhead: TRF2. Note that western blot did not detect either TRF1 or TRF2 in the FBXO47 immunoprecipitate.

(B) Chromosome spreads of *Fbxo47-3FH* KI and control (non-tagged) spermatocytes were immunostained as indicated. Images with enhanced contrast for HA color channel are shown. Note that FBXO47 did not show specific localization pattern to telomeres. We observed no more than background signals, even though contrast for HA images was enhanced.

(C) Structurally-preserved nuclei of spermatocytes were prepared by squashing *Fbxo47* KO testis tubules, and immunostained for LAMIN B, TRF1 and SYCP3. The image acquired at the equator of the spermatocyte nuclei is shown. Note that telomeres attachment to the nuclear envelope was intact in *Fbxo47* KO spermatocytes. Scale bars: 5  $\mu$ m.

(D) The indicated spermatocyte nuclei were immunostained as indicated (left). Telomere clustering in wild-type (n=355) and *Fbxo47* KO (n=345) was scored at 12 day post-partum. The frequency of bouquet stage spermatocytes is shown (right). Statistical significance is shown by N.S.  $p = 0.5025$  (chi square-test).



**Figure 1H****Figure 2E****Figure S3A****Figure 1C****Figure 4B****Supplementary Figure 4. Uncropped images of gels and blots.**

Full-length / uncropped images of agarose gel (Fig1C, Fig4B) and immunoblots (Fig1H, Fig2E, Fig S3A) are shown. Immunoblotted membrane was sequentially reprobbed with different antibodies. For SKP1, H3, TRF1 immunoblots, the same membrane was stripped, cut according to molecular weight marker and reprobbed, so that different proteins could be simultaneously probed with different antibodies.